Sedimentary Controls on Foraminifera Deposition in the Bay of Bengal

A Thesis submitted to the faculty of
San Francisco State University
In partial fulfillment of
the requirements for
the Degree

Master of Science

In

Geosciences

by

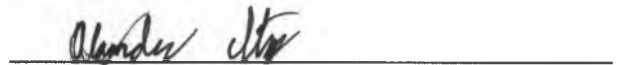Theresa Fritz-Endres

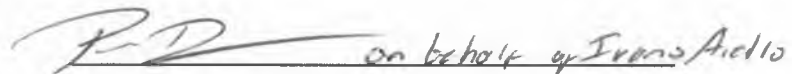San Francisco, California

Summer 2016

CERTIFICATION OF APPROVAL

I certify that I have read Sedimentary Controls on Foraminifera Deposition in the Bay of

Bengal by Theresa Fritz-Endres, and that in my opinion this work meets the criteria for

approving a thesis submitted in partial fulfillment of the requirement for the degree Master

of Science in Geosciences at San Francisco State University.

Petra S. Dekens, Ph.D.
Associate Professor

Alexander Stine, Ph.D.
Associate Professor

on behalf of Ivano Aiello

Ivano Aiello, Ph.D.
Associate Professor

Sedimentary Controls on Foraminifera Deposition in the Bay of Bengal

Theresa Fritz-Endres
San Francisco, California
2016

Recent IODP expeditions to the Bay of Bengal present an excellent opportunity for better understanding the links between terrestrial and oceanographic climate variability over a variety of timescales. However, foraminifera in Bengal fan sediments may have been transported via turbidity currents. Given the variability in SST and SSS between the southern Bay of Bengal (29.0±0.8°C; 33.9 ±0.3‰) and the northern Bay of Bengal where foraminifera may be transported from (28.0±1.4°C; 31.6±0.8‰), it is important to determine the source of foraminifera to the sediment cores before attempting paleoceanographic reconstructions. We present single foraminifera Mg/Ca and $\delta^{18}O$ data from mudline samples of IODP Expedition 354 site U1454 (8.4°N, 85.5°E, 3721 m water depth) near the modern active channel and more likely to be influenced by transport and site U1449 (8.4°N, 88.7°E, 3653 m water depth) far from channel activity. We compare individual *Globigerinoides sacculifer* from these sites to the core-top sample of site 342KL (19°97'N, 90°03'E, 1256 m water depth) located on the continental shelf. Each foraminifera lives ~2-4 weeks and the distribution of 70 to 80 data points therefore reflects the seasonal range of SST and SSS at the location in which the foraminifera calcified. Foraminifera at site far from channel activity reconstruct the modern seasonal SST (-1.0°C difference) and $\delta^{18}O$ (-0.9‰ difference) signal of the southern Bay of Bengal. Foraminifera at site near the active channel reflect the SST (1.3°C difference) and $\delta^{18}O$ (0.4‰ difference) signal also recorded in foraminifera from the continental shelf. This suggests a portion of foraminifera at this site have been transported from the northern Bay of Bengal. Our data shows that foraminifera can be used to reconstruct SST and $\delta^{18}O$ in this complex depositional environment, but caution must be taken when the down-core lithology indicates turbidites and possible sediment transport.

I certify that the Abstract is a correct representation of the content of this Thesis

_____   ___7/19/16___

Chair, Thesis Committee   Date

ACKNOWLEDGEMENTS

TABLE OF CONTENTS

LIST OF FIGURES

LIST OF TABLES

LIST OF APPENDICES

1. Introduction

The uplift of the Himalayas may have strengthened the East Asian monsoon [*Yanai et al.*, 1992; *Zhisheng et al.*, 2001] and contributed to Cenozoic cooling [*Raymo et al.*, 1992] and major climate transitions over the past 10 Ma. International Ocean Drilling Program (IODP) Expedition 354 sites in the Bay of Bengal record Himalayan erosion and oceanographic conditions through the last 10 Ma [*France-Lanord et al.*, 2014]. To test the connections between tectonics, monsoons strength, and oceanographic conditions, it is critical to reconstruct surface ocean conditions though this time period.

Cores recovered from the IODP Expedition 354 present a unique opportunity to link oceanic and terrestrial climate variability. Sediment in IODP Expedition 354 cores includes terrigenous material transported from the Himalayas [*France-Lanord et al.*, 2014] and biogenic material from the overlaying water column or reworked by turbidity flows. The terrigenous sediment records Himalayan erosion [*France-Lanord et al.*, 2014], and coupling this with proxies of sea surface temperature (SST) and sea surface salinity (SSS) recorded by foraminifera has the potential to reconstruct the regional and global response to major phases of Himalayan uplift [*Zhisheng et al.*, 2001].

To take advantage of these unique cores and link oceanic and terrestrial proxy records, we must show that foraminifera based proxies can be used to generate records of local seawater conditions in this complex depositional environment. The chemistry of foraminifera shells is set at the sea surface before shells fall rapidly through the water column [50-200 m/day; *Stoll et al.*, 2007]. Typically, shells preserved in sediment are

estimated to originate from an area of the sea surface directly above and up to a hundred kilometers away [*Siegel and Armstrong,* 2002]. Because the Bengal Fan is influenced by turbidity flows and sediment reworking, we must consider the possibility that the foraminifera may have been transported from the northern Bay of Bengal.

The Bay of Bengal depositional system is the largest in the world [*Curray et al.,* 2003]. Heavy monsoonal precipitation erodes Himalayan source rock and the Ganges and Brahmaputra rivers transport ~1 billion tons of sediment 3000 km to the continental shelf [*Curray et al.,* 1991]. One third of the sediment deposited on the shelf is transported through submarine canyons during times of high sedimentation when glacial activity results in sea-level low-stands and then transported through the active channel by gravity currents to the upper, middle, and lower sub-fan [*Michels et al.,* 1998]. Channel activity is reduced in times of sea-level high-stands and modern time as less sediment reaches submarine canyons and pelagic material accumulates [*Weber et al.,* 2003]. The pelagic material is therefore subject to reworking by transportation activity.

The channel-levee systems that compose the lower fan are made of sediment transported through incised channels. Channel activity has migrated from the Ninetyeast Ridge westward over the past 300 Kyr, leaving three distinct abandoned channels and an active channels running along the middle of the fan [*Curray et al.,* 2003]. Turbidity flows move episodically through meandering active channels and overspill their banks onto bends much like a river [*Curray et al.,* 2003]. These individual sedimentation events form levees composed of graded beds that border the active channels [*Curray et al.,* 2003].

Through time and channel switching this sedimentation process has produced a profile of stacked channel-levee systems present in the lower fan since the Pliocene [*Spiess*, 1998]. IODP Expedition 354 recovered full levee sequences that contain repeated turbidites, coarse material, and debris fragments interbedded with bioturbated hemipelagic units [*France-Lenord et al.*, 2015]. Hemipelagic units are formed by the settling of fine particles and are a mixture of biogenic material and reworked material transported from an upstream source.

To determine if foraminifera record local water conditions we use the fact that the seasonal range of SSS and SST is spatially variable in the Bay of Bengal (Figure 1). The seasonal range of SST and SSS is larger in the northern part of the bay (5°C and 3.0‰, respectively) and smaller in the southern part of the bay where IODP Expedition 354 cores were drilled (1.4°C and 0.7‰, respectively; Figure 1). We measured $\delta^{18}O$ and Mg/Ca on single foraminifera shells taken from cores in the northern and southern bay. The distribution of the data reflects seasonality; a broader distribution of the data would indicate the larger SSS and SST range of the northern bay is recorded, while a narrower data distribution would indicate the much smaller SSS and SST range of the southern bay is recorded.

1.1 Oceanographic conditions

Seasonal monsoonal precipitation and currents produce spatially variable SSS and SST in the Bay of Bengal (Figure 1). Strong winds from the southwest develop the

Southwest Monsoon Current and supply heavy precipitation over the Bay of Bengal and Himalayas June-August (Figure 1; *Schott*, 2009). During June-August high precipitation over the sea surface and fresh water from the Ganges-Brahmaputra drainage basin brings fresher water to the Bay of Bengal [*Lupker et al.*, 2011; *France-Lenord*, 2000] and the Southwest Monsoon Current isolates freshwater in the northern part of the bay and brings saltier Arabian Sea water to the southern part of the bay [*Schott*, 2009]. A seasonal wind reversal establishes the Northeast Monsoon Current and results in less precipitation in January-February, and the Northeast Monsoon Current brings more saline subequatorial water north into the Bay of Bengal [*Rostek et al.*, 1994]. Seasonal precipitation results in a large SSS range (3.0‰; Table 1) in the northern part of the bay [*Levitus*, 1982]. In contrast, monsoonal precipitation does not reach the southern part of the bay and does not experience the same effect of seasonal freshening, resulting in a significantly smaller seasonal SSS range (0.7‰; Table 1) [*Levitus*, 1982].

Seasonal surface water cooling isolated in the northern part of the bay by currents results in a spatially variable SST. Less dense freshwater from the Ganges-Brahmaputra drainage basin produces a shallow seasonal mixed layer which warms in the pre-monsoon period March-June with an increased heat flux and suppressed upwelling [*Unger et al.*, 2003]. In January-February seasonal winds produce a deeper mixed layer in the northern Bay of Bengal and surface water cools rapidly with a decreased heat flux [*Han et al.*, 2001]. This does not occur in the southern part of the bay where the Southwest Monsoonal Current brings warm but dense saltier water from the Arabian Sea June-

August and the Northeast Monsoon Current brings warm but dense subequatorial water January-February. This results in a deeper mixed layer and warmer surface water throughout the year [*Schott*, 2009]. The result is a larger seasonal SST range (5°C) in the northern Bay of Bengal and a smaller SST range (1.4°C) in the southern Bay of Bengal [Table 1; *Levitus*, 1982].

1.2 Foraminifera geochemical proxies

Measurements of $\delta^{18}O$ coupled with Mg/Ca in the same individual foraminifera records the sea water conditions in which the foraminifera shell calcified and are important tools to unravel local salinity and temperature [*Shackleton*, 1974; see Appendix B]. $\delta^{18}O$ in planktonic foraminifera is influenced by global ice volume, local salinity, and temperature and is therefore a combined signal of $\delta^{18}O$ of seawater ($\delta^{18}O_{sw}$), SSS, and SST [*Shackleton*, 1974; *Rohling and Cooke*, 1999]. Because Mg/Ca independently measures temperature, the temperature and $\delta^{18}O_{sw}$ signals in the $\delta^{18}O$ of the foraminifera calcite ($\delta^{18}O_{calcite}$) can be separated [*Mashiotta et al.*, 1999] to record the precipitation-evaporation balance and SSS signal [*Lea*, 2003].

There are several factors that affect Mg/Ca and $\delta^{18}O$ of foraminifera that may influence our ability to reconstruct oceanographic conditions, including species selection,

foraminifera size, and the chamber sampled. Foraminifera migrate through the water column based on their temperature and salinity preferences, which can be unique to the species and life cycle stage of the individual [*Eggins et al.*, 2003; *Lohmann*, 1995]. Foraminifera precipitate calcite in layers that cover their pre-existing shell each time they build a new chamber [*Erez*, 2003] so the shell is composed of chambers with layers of calcite and the size increases throughout the life of the individual [*Reiss*, 1957]. Sampling shells of different sizes and species may indicate individuals calcified within different water masses based on their preferences [*Eggins et al.*, 2003; *Lohmann*, 1995] and would affect the Mg/Ca and $\delta^{18}O$ recorded.

Secondary factors include shell dissolution or precipitation of contaminants and secondary calcification. Partial dissolution of Mg-rich shell components occurs in water that is under-saturated with respect to calcite and leads toward a cold temperature bias in the proxy [*Brown and Elderfield*, 1996; *Dekens et al.*, 2002; *Regenberg et al.*, 2007]. Conversely, precipitation of Magnesium-Manganese (Mn-Mg) rich contaminant phases [*Boyle*, 1983] and accumulation of silicate contaminants can result in elevated Mg/Ca values and bias the SST record toward warmer temperatures [*Barker et al.*, 2003]. Secondary calcification occurs when foraminifera cover their pre-existing shell with a new layer of calcite. Toward the end of their life cycle many foraminifera species deposit layers of calcite as a thick crust. This crust often has different chemical and isotopic compositions in part because it is deposited in deeper water where the chemistry of the

seawater is different from the chemistry of surface waters, so this calcite reflects conditions other than that of the sea surface [*Bé*, 1980; *Mohan et al.*, 2015].

2. Methods

The hemipelagic mudline samples (the top few centimeters of unconsolidated sediment) are the most recently deposited sediment and are influenced by the modern depositional environment [*France-Lenord et al.*, 2015]. IODP site U1454 (Figure 1) is on the western levee of what is likely the only presently active channel [*Hübscher et al.*, 1997; *Curray et al.*, 2003] and consists of hemipelagic calcareous clay influenced by sediment from turbidity flows [*France-Lenord et al.*, 2015]. IODP site U1449 is located ~250 km from the active channel, where the modern sediment is less likely influenced by channel activity [*France-Lenord et al.*, 2015]. We compare the two IODP Expedition 354 sites to the core top of site 342KL on the upper continental shelf of Bangladesh where sediment is composed of hemipelagic mud of mostly marine material [Figure 1; *Pierson-Wickmann et al.*, 2001].

Samples were washed with distilled water over a 63 μm sieve to remove clays. We selected shells of mixed layer dwelling species *Globigerinoides sacculifer* within the 250-355 μm and 355-425 μm size fraction. Prior to analysis, individual foraminifera samples were sonicated in Milli-Q water for 5-10 seconds, rinsed with methanol, dried, and mounted onto carbon tape following *Eggins et al.* [2003].

Mg/Ca was measured in ~70-80 individual foraminifera shells per site using a laser ablation system Photon Machines 193 nm ArF UV excimer laser-ablation system with an ANU HelEx dual-volume laser ablation cell coupled to an Agilent 7700x quadrupole inductively coupled plasma mass spectrometer (LA-ICP-MS) at the University of California Davis (UCD) Stable Isotope Lab. Three to seven spots ~44 μm in diameter were made on the final (F) chamber of individual shells and analyzed for selected isotopes (^{24}Mg, ^{25}Mg, ^{43}Ca, ^{44}Ca, ^{138}Ba, ^{88}Sr, ^{11}B, ^{27}Al, and ^{55}Mn). ^{27}Al and ^{55}Mn were monitored for clay and oxide contamination. A small subset (~10 from each site) of next to final (F1) and two from final (F2) chambers were also analyzed. Values from laser spots were averaged to calculate one mean value per chamber and per individual.

Data acquisition was between 40-60s per spot analysis. The mean Mg/Ca ratio for each profile was calculated by normalizing to the known trace element concentration in the drift-corrected bracketed analyses of the NIST SRM 610 and 612 glass standards at 5Hz and 50% laser fluence [*Jochum et al.*, 2011]. 16 repeat analyses along the same track gave a reproducibility of the mean Mg/Ca of 10.4 ± 0.45 mmol/mol ($\pm 4.3\%$) for NIST 610 and 1.66 ± 0.08 mmol/mol ($\pm 4.8\%$) for NIST 612. Samples were analyzed at 5Hz and 5% and 30-36% laser fluence respectively. We used ^{43}Ca as our internal standard and monitored ^{44}Ca to check for consistency. We also monitored for ^{27}Al and ^{55}Mn to check for surface contamination and termination of shell ablation through to the carbon tape (often seen as a spick in concentration at the end of the profile) [*Fehrenbacher et al.*, 2015].

All data was reduced using a de-spiking routine that includes a noise and washout filter. The noise filter excludes 12 standard deviations above the rolling sample mean and the washout filter accounts for time required for the laser signal to reach the mass spectrometer as a function of the flushing time of the sample cup assuming an exponential laser signal decay constant of 1.17 [*Longerich et al.*, 1996]. Mg and Ca concentrations were obtained by integrating for a mean minor elemental signal using Iolite [*Iolite Software*, 2016].

Following ablation we carefully removed individual shells from the carbon tape with methanol and used the remaining material for $\delta^{18}O$ analysis. ~30-40 individual foraminifera at each site (samples selected to weigh no less than 12 µg) were roasted in vacuum at 375°C overnight to remove residual adhesive and prevent contamination prior to being analyzed. Oxygen and carbon isotopes were measured using an automated carbonate device coupled with a GVI Optima Stable Isotope Ratio Mass Spectrometer (SIRMS) at the UCD Stable Isotope Lab. $\delta^{18}O$ results were calibrated and reported relative to the Vienna Pee Dee Belemnite standard (V-PDB) through an in-house Carrara Marble that has been calibrated against NBS-19 (UCD-SM92), which has a long-term internal reproducibility of 0.08‰. The reproducibility (σ) for $\delta^{18}O$ based on 36 measurements of the UCD-SM92 standard throughout the analysis was -1.94 ± 0.11‰ (± 5.7%).

In addition to measuring $\delta^{18}O$ and Mg/Ca, we used the Zeiss Ultra 55 Field Emission Scanning Electron Microscope (FE-SEM) at San Francisco State University

(SFSU) to examine individual shells for signs of contamination or dissolution. The ultrastructure of foraminifera calcite shells break down progressively with increasing carbonate dissolution, even above the lysocline [*Dittert and Henrich*, 2000]. Signs of dissolution in most of the individuals would indicate that samples have remained in waters under-saturated with respect to calcite. 9 samples from core U1454 (southern-active), 10 samples from U1449 (southern-not active), and 8 samples from 342KL (northern) were selected, fastened onto SEM stubs with carbon paint and gold coated prior to analysis. Individuals were selected blindly to reduce bias of selecting more or less preserved shells.

3. Results/Discussion

The goal of the project is to determine if foraminifera recovered from IODP Expedition 354 sites in the southern Bay of Bengal record the overlying water conditions or water conditions of the northern Bay of Bengal. We calculate the mean and distribution (1σ) of local oceanographic SST (SST_{insitu}) at the location of 342KL site (northern) and Expedition 354 sites (southern) using 780 data points from months SST data collected over 1950-2015 in a 1° x 1° grid box around each site [*Hadley Center*, 2015]. The regional monsoon results in a larger seasonal temperature and salinity range in the northern Bay of Bengal site ($28.8 \pm 1.1°C$ and $32.9 \pm 0.4‰$; *Hadley Center*, 2015)

compared to the southern sites (29.1 ± 0.8°C and 34.1 ± 0.3‰; *Hadley Center*, 2015) and the means of the two locations are significantly different (p < 0.01, 2-sample student's t test, 2-tail, Figure 1). These oceanographic differences between the regions should be reflected in the distribution of the geochemistry of foraminifera that precipitate their shells in these regions. In order to test the hypothesis that the geochemical data of two groups are equal to one another we use a two-tailed two sample student's t-test throughout the analysis (see Appendix F).

The seasonal distribution of temperature and salinity at the location where individual foraminifera formed their shells is reflected in the distribution of Mg/Ca and $\delta^{18}O$ values [*Wit et al.*, 2010]. However, biological factors affect how foraminifera incorporate elements and isotopes from seawater [*Erez et al.*, 1991], and post depositional alterations can change the primary Mg/Ca and $\delta^{18}O$ signal in the calcite [*de Villiers*, 2005; *Anjos-Zerfass et al.*, 2011]. These biological factors (including species, size fraction, and chamber selected) and post-depositional processes (dissolution and contamination) could introduce uncertainty that exceeds the oceanographic signal [*Wit et al.*, 2010; *Sadekov et al.*, 2009; *Marr et al.*, 2011]. We therefore first consider the potential impacts of these processes on single foraminifera data before considering what the data implies about the source of foraminifera.

3.1 Effect of contaminants on Mg/Ca and $\delta^{18}O$

Precipitation of Mn-Mg rich contaminant phases and accumulation of silicate contaminants can result in elevated Mg/Ca values and bias the SST record toward warmer temperatures [*Boyle*, 1983; *Barker et al.*, 2003]. For bulk foraminiferal analyses an oxidative and reductive cleaning procedure is used to remove the potential bias of Mn over-coating and silicate infill [*Boyle*, 1981; *Barker et al.*, 2003]. This cleaning technique leads to significant sample loss and is difficult to perform on single specimens [*Barker et al.*, 2003; *Wit et al.*, 2010]. Consistent with other studies using single foraminifera we sonicated 19 *G. sacculifer* (250-355 μm) from site U1454 (southern-active) in Milli-Q water, and preformed a methanol rinse and sonication in Milli-Q water on all other samples [*Wit et al.*, 2010; *Marr et al.*, 2011]. Mg/Ca values of the 19 samples that were only sonicated in Milli-Q have a mean of 6.4 ± 1.8 mmol/mol and the remaining 77 samples that underwent an additional methanol rinse have a mean of 5.7 ± 1.6 mmol/mol. The two sample preparations do not have significantly different Mg/Ca values ($p = 0.16$, 2-sample student's t test, 2-tail). The difference between the means is 0.7 mmol/mol and implies a temperature difference of ~ 6 °C which may mask true temperature signal. For this reason we analyze samples for signs of contamination.

We accessed individual shells for signs of Mn and Mg rich over-coatings and clay infill using a SEM. Clay infill in pores and crusted over-coating of calcite indicates the presence of contaminants [*Anjos-Zerfass et al.*, 2011]. Imaging from a subset of samples from each study site (~27 total) reveals some clay infilling in pores, but there were no

signs of crusted over-coatings of calcite (Figure 3 panel A2). If higher Mg/Ca are due to Mn and Al contamination phases then we would expect to see a relationship between Mn/Ca and Mg/Ca and/or Al/Ca and Mg/Ca. There is no significant correlation between Mn/Ca and Mg/Ca (r^2 = 0.07) and only a weak correlation between Al/Ca and Mg/Ca (r^2 = 0.23) for all samples (Figure S2). When we exclude 7 samples that have Mn/Ca > 2 mmol/mol and 12 samples that have Al/Ca > 10 mmol/mol this correlation disappear entirely (r^2 < 0.01 and = 0.09 for Mn/Ca and Al/Ca, respectively) (Figure S2). Samples with Mn/Ca > 2 mmol/mol and Al/Ca > 10 mmol/mol were removed from all further interpretations. The remaining samples include 67 *G. sacculifer* from site U1454 (southern-active), 65 *G. sacculifer* from site U1449 (southern-not active), and 79 *G. sacculifer* from site 342KL (northern).

3.2 Mg/Ca of different shell chambers

Foraminifera add chambers sequentially as they grow, and the Mg/Ca ratio of chambers precipitated during growth may differ [*Marr et al.*, 2011]. For example, *G. ruber* records increasing Mg/Ca ratios with distance from the F chamber [*Wit et al.*, 2010]. This could be due to ontogenetic effects in which changes in growth rate through the foraminifera's life stages have an important effect on Mg/Ca [*Kroon and Darling*, 1995; *Bijma et al.*, 1998]. The F chamber is the last to grow so it samples the part of the water column where the foraminifera lived during its final stage of life, while the F1 and F2 chambers represent a composite of different life stages [*Bé et al.*, 1979; Figure 3,

panel A2]. Previous single foraminifera studies show no significant difference between the F chamber in individual *G. sacculifer* and the whole shell Mg/Ca ratio ($p > 0.05$, paired sample student's t test, 2-tail), however there are statistically significant differences between the F and F1 and F2 chambers ($p \ll 0.05$, paired sample student's t test, 2-tail) [*Brown and Elderfield*, 1996; *Fehrenbacher*, in prep]. Yet, not enough studies have been done to verify these results. We measured F and F1 chambers of 29 *G. sacculifer* and additionally F2 chambers of 12 of these samples and calculated a two-chamber and a three-chamber mean (Figure S4; Table S2). The *G. sacculifer* F chamber records only slightly higher Mg/Ca than two-chamber and three-chamber mean, but the difference is not significant ($p = 0.98$ and 0.89, respectively, 2-sample student's t test, 2-tail). The small difference between mean values from F and F1 and F2 chambers are also not significant ($p = 0.07$, 2-sample student's t test, 2-tail) and neither is the variance between chambers ($p = 0.19$, F-test, 2-tailed). Using just the F chamber should not affect seasonal reconstruction as the F chamber mean is not significant difference from the shell mean, and just this chamber is selected for the rest of the analysis.

3.3 Mg/Ca of different shell size fractions

Differences in seasonal preferences, depth habitat, or ontogenetic effects throughout life stages can significantly change the Mg/Ca [*Richey et al.*, 2012] and $\delta^{18}O$ recorded by foraminifera from different size fractions [*Bouvier-Soumagnac and Duplessy*, 1985; *Bemis et al.*, 1998; *Spero and Lea*, 1996; *Elderfield et al.*, 2002]. To test

if the size of foraminifera affects the Mg/Ca recorded we compare Mg/Ca of 67 *G. sacculifer* from the 250-355 μm size fraction to 30 *G. sacculifer* from the 355-425 μm size fraction from site U1454 (southern-active) and 65 *G. sacculifer* from the 250-355 μm size fraction and 12 *G. sacculifer* from the 355-425 μm size fraction from site U1449 (southern-not active) (Figure S5). There is no significant difference between the 250-355 μm and 355-425 μm size fractions at site U1454 nor at site U1449 ($p = 0.37$ and 0.05, respectively, 2-sample student's t test, 2-tail). Although this is encouraging, sieving may not be the best way to constrain shell size because the sieve often prevents smaller shells or allows larger shells to pass through [*Elderfield et al.*, 2002].

We measured the length of the individual shells at their longest axis and find there is a weak positive relationship between Mg/Ca and the length of shell from site U1454 (southern-active), site U1449 (southern-not active), and site 342KL (northern) ($r^2 = 0.02$, 0.09, 0.10, respectively, Figure S6). Surprisingly, within the 250-355 μm size fraction 9 individuals from site U1454 and 5 individuals from site U1449 and 2 individuals from 342KL are > 425 μm. Within the 355-425 μm size fraction 7 individuals from site U1454 and 2 individuals from site U1449 are < 355 μm. The Mg/Ca difference between 250-450 μm and 450-650 μm samples at site U1454 is 1.1 ± 1.2 mmol/mol ($p < 0.01$, 2-sample student's t test, 2-tail) and at site U1449 is 1.6 ± 1.3 mmol/mol ($p < 0.01$, 2-sample student's t test, 2-tail), which represents an increase in SST of ~15 and ~18°C (at site U1454 and site U1449, respectively). This difference in temperature is consistent with a seasonal influence (SST range is 1.4°C; Figure 1) as larger *G. sacculifer* are more likely

to grow in warmer water [*Spero and Lea*, 1993], but inconsistent with a depth habitat influence (~2°C in 75 m) as *G. sacculifer* are more likely to add calcite in colder deeper water during final life stages. However, the magnitude of the Mg/Ca implied temperature difference is larger than any natural oceanographic variability. This implies that Mg/Ca data are affected by Mg incorporation occurring not at thermodynamic equilibrium and an increase in Mg/Ca with test size is consistent with larger individuals incorporating more Mg than smaller individuals from the same site [*Elderfield et al.*, 2002]. This stresses the importance of using a narrow size range to reduce the effect of biologic or kinetic factors on size [*Elderfield et al.*, 2002]. We choose to interpret Mg/Ca data from only foraminifera that are 250-450 μm based on shell length not size fraction. The remaining samples include 65 *G. sacculifer* from site U1454, 63 *G. sacculifer* from site U1449, and 77 *G. sacculifer* from site 342KL.

3.4 Converting Mg/Ca to SST

     G. sacculifer F chamber (250-450 μm) mean Mg/Ca of 65 samples from site U1454 (southern, active; 5.7 ± 1.4 mmol/mol) is significantly different from the mean of 63 samples from site U1449 (southern not active; 4.9 ± 1.5 mmol/mol) ($p < 0.01$, 2-sample student's t test, 2-tail) and the mean of 77 samples from site 342KL (northern; 6.5 ± 2.0 mmol/mol) ($p < 0.01$, 2-sample student's t test, 2-tail) (Figure 2; Table 2). The mean Mg/Ca from site U1449 is also significantly different from site 342KL ($p < 0.001$, 2-sample student's t test, 2-tail). The variance, which statistically describes the

distribution of the data, is not statistically different between U1454 and U1449 sites (p = 0.92, F-test, 2-tailed). However, both of the southern Bay of Bengal sites have variances that are statistically different form the northern 342KL site (p < 0.01 for U1454 and U1449, F-test, 2-tailed).

To determine if foraminifera Mg/Ca record local oceanographic conditions, we must convert Mg/Ca to SST. There are several established calibrations, which are based on culturing, plankton tows, sediment trap, and core-top samples [*Elderfield and Ganssen, 2000*; *Dekens et al.* 2002; *Anand et al.*, 2003; *Regenberg et al.*, 2009]. All calibrations describe the relationship between Mg/Ca and SST as an exponential equation and take the form of:

$$Mg/Ca = B * e^{A * T} \qquad [1]$$

where T is the calcification temperature (°C) and A and B are constants. We compare calculated Mg/Ca SST ($SST_{Mg/Ca}$) using several calibration equations to local SST_{insitu} for each site (Table 3) and consider the merits of using sediment trap studies that include a seasonal component or core-top studies that consider the effect of dissolution.

After foraminifera are deposited on the sea floor the shells can experience dissolution of calcite, which preferentially removes Mg^{2+} and lowers shell Mg/Ca, biasing the SST estimates to colder temperatures [*Brown and Elderfield*, 1996; *Dekens et al.*, 2002]. Some calibration equations include a correction factor based on core depth or site specific carbonate ion concentration to correct for this bias [*Dekens et al.*, 2002; *Regenberg et al.*, 2006]. IODP Expedition 354 sites (southern) are bathed in water that is

near the saturation horizon (ΔCO_3^{2-} = 24 µmol/kg; WOCE data and the USGS CO_2 Calculator [*Robbins et al.*, 2010]; see Appendix E) and the lysocline (at ~3800 m in the equatorial Indian Ocean [*Peterson and Prell*, 1985]). Although the study sites are shallower than the lysocline, partial dissolution of foraminifera may begin when ΔCO_3^{2-} concentration is ~18 to 26 µmol/kg at depths of ~2500-3000 m [*Regenberg et al.*, 2006]. The critical ΔCO_3^{2-} is the species-specific ΔCO_3^{2-} concentration level where Mg^{2+} removal begins and is 22.1 µmol/kg for *G. sacculifer* based on studies in the Atlantic [*Regenberg et al.*, 2006]. ΔCO_3^{2-} at all of our sites is near the critical ΔCO_3^{2-} specified for *G. sacculifer* and depth at all our sites approaches the regional lysocline. Therefore the effect of dissolution on our samples must be considered.

Dissolution corrections of *Dekens et al.* [2002] and *Regenberg et al.* [2006] based on ΔCO_3^{2-} and core depth yield average SST estimates that are unrealistically warm compared to local SST_{insitu} (Table 3) at sites U1454 (southern-active) and 342KL (northern). *Dekens et al.* [2002] and *Regenberg et al.* [2006] depth corrections suggest $SST_{Mg/Ca}$ that are more similar to SST_{insitu} at site U1449 (southern-not active) and much warmer than SST_{insitu} at site U1454 (southern-active). This suggests Mg/Ca may be influenced by dissolution at site U1449 while not significantly impacting individuals at site U1454 nor at site 342KL.

We examined 8-10 shells from each site using SEM to assign a preservation stage to each shell after the dissolution index of *Dittert and Henrich* [2000]. Features such as reduced spine bases, sheeted or removed surface layers, frayed pores, formation of

cracks, and rounded crystalline structures indicates shell dissolution [*Dittert and Henrich*, 2000]. SEM analysis shows that 8 of 9 shells from site U1454 (southern-active) and all of 8 shells from 342KL (northern) are well preserved (Figure 3). Samples have well preserved to slightly reduced spine bases (Figure 3 panel A1), preserved shell layers (panel A2), smooth inter-pore areas, round to funneled pores, high to slightly reduced ridges, and sharp to weakly rounded edges of the crystal structures (panel A3). At site U1449 7 of the 10 shells show signs of dissolution with no spines and reduced bases (Figure 3 panel B1), sheeting or partial dissolution of the surface layer (panel B2), round to funneled pores, slightly reduced to reduced ridges, and weakly to slightly rounded crystals (panel B3). SEM work suggests samples from site U1454 are better preserved than samples from site U1449.

SEM analysis and the fact that the dissolution corrected calibration results in $SST_{Mg/Ca}$ that more closely resembles the SST_{insitu} (Table 3) is evidence that foraminifera at site U1449 (southern-not active) have undergone some dissolution. Because there is no visible evidence for dissolution in the SEM images at site U1454 (southern-active) and site 342KL (northern), and because using a dissolution correction calibrations yield $SST_{Mg/Ca}$ estimates that are unrealistically warm at these locations (Table 3), we chose not to apply a dissolution correction to these sites. We also do not apply a dissolution correction calibration to calculate $SST_{Mg/Ca}$ at site U1449. We have no reason to think sites U1454 and U1449 are influenced by significantly different core depth and ΔCO_3^{2-}. Additionally, our goal is to compare values between sites and using different calibration

equations would introduce a bias. For this reason we chose not to apply a dissolution correction calibration to calculate $SST_{Mg/Ca}$ for any of our sites.

We find that applying the *Anand et al.* [2003] calibration:

$$Mg/Ca = 0.38\ (\pm\ 0.02) * e^{\ 0.090\ (\pm\ 0.003)\ * \text{SST}}$$ [2]

to our individual *G. sacculifer* (250-450 µm) yields SST estimates closest to modern SST (Table 3). The *Anand et al.* [2003] calibration used 10 planktonic species and one size fraction (350-500 µm) closest to the size range we chose to analyze (250-450 µm). Species were sampled from sediment traps in the Sargasso Sea collected bimonthly over 6 years [*Anand et al.*, 2003]. This is in contrast to the *Regenberg et al.* [2009], *Elderfield and Ganssen* [2000], and *Dekens et al.* [2002] equations, which are based on core-tops. Sediment trap studies have the advantage of knowing the time of year of foraminiferal growth together with the oceanographic conditions over several seasonal cycles [*Anand et al.*, 2003]. The *Anand et al.* [2003] calibration is therefore more likely to capture the distribution of possible values throughout the year, which is particularly useful in this study.

The calibration of *Anand et al.* [2003] converts Mg/Ca to a mean SST that is within 1°C of SST_{insitu} at IODP Expedition 354 sites and may overestimate SST at site 342KL. The calibration of *Regenberg et al.* [2009] suggests a mean that is colder than SST_{insitu} at IODP Expedition 354 sites and the *Elderfield and Ganssen* [2000] equation suggests unrealistically cold SST (Table 3). Because there is no dissolution correction, estimated temperatures at site U1449 (southern-not active) are colder than those using the

corrections of *Dekens et al.* [2002] and *Regenberg et al.* [2006] and slightly colder than SST$_{insitu}$. However estimates of SST given by the *Anand et al.* [2003] equation are within the accuracy of Mg/Ca paleothermometry of $\pm$ 1.2-1.4°C [*Elderfield and Ganssen*, 2000; *Dekens et al.* 2002; *Anand et al.*, 2003] and are appropriate to use for this study.

3.5 Monte Carlo Simulation of SST$_{Mg/Ca}$

To determine if foraminifera at IODP Expedition 354 sites (southern) record local water conditions or water conditions of the northern Bay of Bengal we compare the mean and variance of single foraminifera SST$_{Mg/Ca}$ estimates from site U1454 on the modern active channel, where active transport of foraminifera is more likely, to site U1449 far away from the modern active channel, and site 342KL in the northern Bay of Bengal (Figure 1). The distribution of foraminifera Mg/Ca values reflects the SST signal at the location where the shells were precipitated together with uncertainty in the analysis, biologic and kinetic calcification variability of foraminifera, post-depositional effects, and a potential bias due to transport, along with other factors.

The mean of the SST$_{Mg/Ca}$ values from site U1454 (southern-active) is between that of sites U1449 (southern-not active) and 342KL (northern) (Figure 4; Table 4) and is statistically different from both ($p < 0.01$ and < 0.02, respectively, 2-sample student's t test, 2-tail). The mean SST$_{Mg/Ca}$ from site U1449 are statistically different from site 342KL ($p < 0.01$, 2-sample student's t test, 2-tail). The variance, which statistically describes the distribution of the data, at site U1454 is not statistically different from the

variance at site U1449 nor site 342KL (p = 0.10, F-test, 2-tail). The variance of $SST_{Mg/Ca}$

at site U1449 is also not statistically different from site 342KL (p = 0.99, F-test, 2-tail).

The comparison of the means and variance at the three different sites suggests that

foraminifera $SST_{Mg/Ca}$ estimates from site U1454 are influenced by both the local

oceanographic conditions and the SST signal recorded in the northern Bay of Bengal.

Our goal is to test whether $SST_{Mg/Ca}$ at each site is consistent with unbiased

sampling of the local SST_{insitu} (data from surrounding 1° x 1° grid box at each site

location; *Hadley Center*, 2015). To do this we build a distribution for the difference

between $SST_{Mg/Ca}$ and SST_{insitu} under the null hypothesis that $SST_{Mg/Ca}$ represents random

samples from the distribution of SST_{insitu}. $SST_{Mg/Ca}$ at our sites have a much larger

distribution (1σ) than the oceanographic distribution (1σ) of SST (Figure 4). In fact, the

variance of $SST_{Mg/Ca}$ at our sites is ~ 9 times greater than the variance of the

oceanographic data and the means are significantly different for all sites (p < 0.01, 2-

sample student's t test, 2-tail). Because there is such a large uncertainty in the $SST_{Mg/Ca}$

analysis we build a distribution for the difference between $SST_{Mg/Ca}$ and SST_{insitu} using a

Monte Carlo simulation to sample the SST_{insitu} data. We randomly sample with

replacement the SST_{insitu} 65 times from site U1454 values, 63 times from site U1449

values, and 77 times from site 345KL values, consistent with the number of foraminifera

used at each site, and add Gaussian noise with an amplitude equal to the variance of the

$SST_{Mg/Ca}$ in order to simulate the measurement noise. Within each set of random sample

draws we calculate a mean value. We repeat this sampling procedure 10,000 times to

create a distribution of possible SST_{insitu} values recorded by the foraminifera population at each site that is a more realistic description of the population uncertainty. We then calculate the difference between the mean of $SST_{Mg/Ca}$ and the Monte Carlo simulation of SST_{insitu} (SST_{MC}) signal with a noise amplitude consistence with the variance of $SST_{Mg/Ca}$ minus the variance of SST_{insitu} (Δmean and Δvariance; Figure 5).

The mean $SST_{Mg/Ca}$ from site U1449 is not statistically different from the SST_{MC} and the mean $SST_{Mg/Ca}$ from site U1454 records slightly warmer temperatures than SST_{MC}, while the mean $SST_{Mg/Ca}$ from site 342KL records much warmer temperatures than SST_{MC} (Figure 5). The warmer temperature recorded at site 342KL may be related to foraminifera seasonal preference. Sediment traps in the northern and central Bay of Bengal show that planktonic foraminifera flux exhibits a bi-modal distribution pattern related to the monsoon [*Stoll et al.*, 2007; Figure S7; *Zaric et al.*, 2005]. The highest fluxes of foraminifera are recorded during the Southwest Monsoon (May-August) when SST are warmer at site 342KL [*Guptha et al.*, 1997; *Unger et al.*, 2003]. Fluxes during the Northeast Monsoon (January-February) are elevated but not as high as seen during the Southwest Monsoon [*Unger et al.*, 2003]. Because the seasonal distribution is large in the northern part of the bay and small in the southern part of the bay (Figure 1), sampling from the warmest months at each location could change the SST sampled by the foraminifera significantly in the northern bay and very little in the southern bay.

To simulate foraminifera seasonal preference, we used the same Monte Carlo approach as before, but only random sample from SST_{insitu} values from May-August. We

calculate a distribution of possible SST_{MC} means and a distribution of possible Δmean between SST_{MC} and the $SST_{Mg/Ca}$ (Figure 6). We find that the difference between SST_{MC} and $SST_{Mg/Ca}$ means (Δmean) is reduced (1°C difference) at site 342KL compared to the previous simulation and is not significantly changed (~0.2°C difference) at U1454 and U1449 site locations. This indicates that samples at site 342KL could be recording mostly warm months due to seasonal variability in foraminifera flux. This seasonal bias cannot be replicated at site U1454, suggesting that samples from site U1454 are warmer because they are recording a partial signal from further north.

Samples from site U1454 may be a mixture of locally derived samples and samples derived from further north. We use a weighted random sampling approach to simulate the portion of samples needed from each 342KL and U1449 sites to replicate the mean of $SST_{Mg/Ca}$ values from site U1454. We assume that samples from site U1449 are locally derived from the southern bay and that samples from site 342KL are derived from that northern location. We calculate a distribution of possible sample means and a distribution of Δmean between the Monte Carlo simulated values and $SST_{Mg/Ca}$ from site U1454 (Figure 7). We test several sampling ratios and find that the Δmean is likely to be ~ 0°C when we sample from sites U1449 and 342KL in the proportion 1:1.5.

3.6 Foraminifera $\delta^{18}O$ and $\delta^{18}O$ of seawater

$\delta^{18}O$ of foraminifera calcite ($\delta^{18}O_{calcite}$) records both temperature and the oxygen isotopic composition of seawater ($\delta^{18}O_{sw}$) [*Rohling and Cooke*, 1999]. Given that salinity

and $\delta^{18}O_{sw}$ are both controlled by changes in precipitation and evaporation balance [*Duplessy*, 1982], the seasonality of both SST and SSS of the location in which foraminifera precipitated their shells will be recorded in $\delta^{18}O_{calcite}$. We measured $\delta^{18}O$ in 37 individual *G. sacculifer* (250-450 μm) from site U1454, 20 from site U1459, and 27 *G. sacculifer* (250-450 μm) from site 342KL. The mean of $\delta^{18}O_{calcite}$ values from site U1454 (-2.2 ± 0.3‰) is between values from site U1449 (-1.7 ± 0.5‰) and site 342KL (-2.6 ± 0.3‰) (Figure 2; Table 2). $\delta^{18}O_{calcite}$ from site U1454 is significantly different from both sites U1449 and 342KL ($p < 0.01$, 2-sample student's t test, 2-tail). The mean of $\delta^{18}O_{calcite}$ values from site U1449 is significantly different from site 342KL ($p < 0.01$, 2-sample student's t test, 2-tail). The variance of $\delta^{18}O_{calcite}$ values from site U1454 is not significantly different from both sites U1449 and 342KL ($p = 0.50$ and 0.42, respectively, F-test, 2-tail) and the variance of $\delta^{18}O_{calcite}$ values from site 342KL is significantly different from site U1449 ($p < 0.01$, F-test, 2-tail).

Because Mg/Ca and $\delta^{18}O$ are measured in the same sample material, the distribution of the single foraminifera data will reflect seasonal variability in both SST and SSS. $\delta^{18}O_{calcite}$ are paired with $SST_{Mg/Ca}$ estimates to calculate $\delta^{18}O_{sw}$ using the calibration of Shackleton [1974]:

$$SST = 16.9 - 4.38\ (\delta^{18}O_{calcite} - \delta^{18}O_{sw}) + 0.1\ (\delta^{18}O_{calcite} - \delta^{18}O_{sw})^2 \quad [3]$$

$\delta^{18}O_{calcite}$ values were converted from V-PDB to V-SMOW with a correction factor of 0.27‰ [*Hut*, 1987].

Because the foraminifer $\delta^{18}O_{sw}$ estimate is derived from $SST_{Mg/Ca}$ and $\delta^{18}O_{calcite}$, the error associated with these values are propagated in the $\delta^{18}O_{sw}$ reconstruction. The distribution (σ) in $SST_{Mg/Ca}$ is between 3.2 and 2.7°C (Table 3). This distribution is effected only negligibility by the analytic error ($\sim \pm 0.5$°C based on NIST 610 and NIST 612 standard reproducibility) and more prominently by the accuracy of the calibration equation used to convert Mg/Ca to SST (± 1.2°C, [*Anand et al.*, 2003]) and the distribution (σ) of values of three to seven sample spots within an individual shell ($\pm$ 1.3°C). The accumulation of the uncertainties from these three sources contributes $\sim \pm$ 1.8°C to the distribution (σ) in $SST_{Mg/Ca}$. The distribution (σ) in $\delta^{18}O_{calcite}$ is between 0.3 and 0.5‰ (Table 2). The analytical error contributes only minimally ($\sim \pm 0.11$‰ based on UCD-SM92 standard reproducibility) and the rest of the distribution (σ) may be attributed to factors effecting foraminifera calcification and SST_{insitu} and $\delta^{18}O_{sw}$. The error in both the $SST_{Mg/Ca}$ and $\delta^{18}O_{calcite}$ estimates propagates when used to calculate $\delta^{18}O_{sw}$ and the accumulation of error is $\sim \pm 7.8\%$ of the mean or $\sim \pm 0.17$‰. This error may mask real variability in the $\delta^{18}O_{sw}$ record. While we assign absolute $\delta^{18}O_{sw}$ to foraminifera values, we discuss relative magnitude of changes over definitive $\delta^{18}O_{sw}$ reconstruction.

Single shell $\delta^{18}O_{calcite}$ is influenced by $\delta^{18}O_{sw}$, which is distinct between southern and northern Bay of Bengal locations. The annual mean $\delta^{18}O_{sw}$ is 0.32‰ at IODP Expedition 354 sites and -0.55‰ at the northern Bay of Bengal site based on 21 data points from Mar-1991, Jan-1994, Sep-2002, and Apr-2003 in a 5° x 5° grid box around

each site location available from the GISS Global Seawater Oxygen-18 Database [*Schmidt et al.*, 1999]. The mean of foraminifera derived $\delta^{18}O_{sw}$ is 0.45‰ greater than local $\delta^{18}O_{sw}$ at site U1454, 0.65‰ greater than local $\delta^{18}O_{sw}$ at site U1449, and 1.08‰ greater than local $\delta^{18}O_{sw}$ at site 342KL (Figure S9). One cause of this offset may be the error associated with the limited seasonal data available. The analytical error in the measurement of $\delta^{18}O_{sw}$ in surface water samples is 0.05‰ [*Delaygue et al.*, 2001; *Singh et al.*, 2010] and the standard error of the data points we used to calculate the annual mean $\delta^{18}O_{sw}$ is 0.10‰ and together contributes an error of 0.11‰. The rest of the offset is likely due to the weak relationship between $\delta^{18}O_{calcite}$, $SST_{Mg/Ca}$, and $\delta^{18}O_{sw}$. While foraminifera derived $\delta^{18}O_{sw}$ is offset from local $\delta^{18}O_{sw}$, values from site U1449 and 342KL do follow the trend of local $\delta^{18}O_{sw}$; that is values from site U1449 record higher $\delta^{18}O_{sw}$ and values from site 342KL record lower $\delta^{18}O_{sw}$ as is expected if they are recording local $\delta^{18}O_{sw}$.

We compare foraminifera $\delta^{18}O_{sw}$ from sites U1454, U1449, and 342KL and observe that site U1454 values are between values from site 342KL and site U1449. The mean of $\delta^{18}O_{sw}$ values from site 342KL is 0.24‰ less than that of site U1454 and 0.44‰ less than that of site U1449. The values from site U1454 are not significantly different from site U1449 ($p = 0.28$, 2-sample student's t test, 2-tail) nor are they different from site 342KL ($p = 0.15$, 2-sample student's t test, 2-tail). Values from site 342KL are significantly different from site U1449 ($p < 0.05$, 2-sample student's t test, 2-tail).

4. Implications for sources of foraminifera in IODP Expedition 354 sites

There is a significant difference in the distribution of Mg/Ca and $\delta^{18}O$ of *G. sacculifer* (250-450 μm) calcite from site U1454 on the modern active channel and site U1449 on the same transect, but far away from channel activity. Mg/Ca values from site U1454 are between values from site U1449 which are lower and site 342KL which are higher. This suggests that foraminifera from site U1454 are influenced by a combination of the seasonal signal that is reflected in Mg/Ca of foraminifera from site U1449 and the seasonal signal reflected in Mg/Ca of foraminifera from site 342KL.

When we convert Mg/Ca to SST, values from site U1449 are lower than local modern oceanographic SSS (-1.0°C difference) within calibration error. Lower values may be due to partial dissolution of shells, which is evident in SEM analysis. $SST_{Mg/Ca}$ values from site U1454 are higher than local SST_{insitu} (by 0.9°C) and are not statistically different from $SST_{Mg/Ca}$ values from site 342KL. The $SST_{Mg/Ca}$ estimates can be used to reconstruct local seasonal SST at site U1449 far from channel activity, while $SST_{Mg/Ca}$ values at site U1454 are influenced by values from further north.

We convert $\delta^{18}O_{calcite}$ to $\delta^{18}O_{sw}$ using the $SST_{Mg/Ca}$ from the same individual foraminifera. Calcite derived $\delta^{18}O_{sw}$ from sites U1449 and 342KL, which are most likely to reflect local conditions, are lower than local oceanographic $\delta^{18}O$ (-1.1‰ difference and -1.8‰ difference, respectively), likely due to the weak relationship between $\delta^{18}O_{calcite}$, $SST_{Mg/Ca}$, and $\delta^{18}O_{sw}$. Site U1454 $\delta^{18}O_{sw}$ values fall between values from site 342KL and site U1449 and are not statistically different than values from site 342KL. This is

evidence that values from site U1454 are influenced by $\delta^{18}O_{sw}$ from 342KL and U1449 sites.

5. Conclusions

IODP Expedition 354 cores offer an opportunity to develop high quality and high-resolution records of the change in the monsoon with Himalayan uplift and glacial/interglacial transitions since the Miocene [*France-Lanord et al.*, 2015]. The surface water temperature and salinity record derived from foraminifera is linked to the intensity of monsoon precipitation, which may be influenced by glacial/interglacial cycles and the uplift of the Himalayas [*Yanai et al.*, 1992; *Zhisheng et al.*, 2001]. However, core sites are subject to episodic turbidity flows and foraminifera shells may have been transported with turbidity currents and record the distinct seasonal signal of the northern Bay of Bengal. In order to attempt paleoceanographic reconstruction we must first identifying the source of foraminifera to the sediment cores.

We use paired Mg/Ca and $\delta^{18}O$ measurements to reconstruct SST and $\delta^{18}O$ of seawater at the location foraminifera calcified. We find that foraminifera sampled from a core site on the modern active channel and foraminifera from the continental shelf partially record the same seasonal oceanographic signal. This seasonal signal is reflected independently in Mg/Ca and $\delta^{18}O$ and is strong evidence that a portion of foraminifera at

the active channel site have been transported from the northern Bay of Bengal. Foraminifera from a core site far from channel activity reconstruct the seasonal oceanographic SST and $\delta^{18}O$ signal of the southern Bay of Bengal. Our data shows that foraminifera can be used to reconstruct SST and $\delta^{18}O$ in this complex depositional environment, but caution must be taken when the down-core lithology indicates turbidites and other evidence of sediment redeposition.

6. References

Anand, P., Elderfield, H., and Conte, M.H. (2003), Calibration of Mg/Ca thermometry in planktonic Foraminifera from a sediment trap time series, Paleoceanography, 18(2), 1050, doi:10.1029/2002PA000846.

Anjos-Zerfass, G. D. S., Chemale, F. J., and Moura, C. A. (2011), Post-depositional effects on the microstructure and stable isotopes composition of planktic foraminiferal tests from the Miocene of the Pelotas Basin, south Brazilian continental margin. Revista Mexicana de Ciencias Geológicas, 28(1), 92-104.

Arbuszewski, J., Kaplan, A., and Farmer, E. C. (2010), On the fidelity of shell-derived $\delta^{18}O$ seawater estimates. Earth and Planetary Science Letters, 300(3), 185-196, doi:10.1016/j.epsl.2010.10.035.

Barker, S., Greaves, M., and Elderfield, H. (2003). A study of cleaning procedures used for foraminiferal Mg/Ca paleothermometry. Geochemistry, Geophysics, Geosystems, 4(9), doi:10.1029/2003GC000559.

Bé, A., Hemleben, C., Anderson, O.R., and Spindler, M. (1979), Chamber Formation in Planktonic Foraminifera. Micropaleontology 25 (3), 294–307, doi:10.2307/1485304.

Bé, A. (1980), Gametogenic Calcification in a Spinose Planktonic Foraminifera, *Globigerinoides Sacculifer*, Marine Micropaleontology, 5(3), 283–310, doi:10.1016/0377-8398(80)90014-6.

Bemis, B. E., Spero, H. J., Bijma, J. and Lea, D. W. (1998), Reevaluation of the oxygen isotopic composition of planktonic foraminifera: Experimental results and revised paleotemperature equations, Paleoceanography, 13(2), 150–160, doi:10.1029/98PA00070.

Bijma, J., Hemleben, C., Huber, B. T., Erlenkeuser, H., & Kroon, D. (1998). Experimental determination of the ontogenetic stable isotope variability in two morphotypes of *Globigerinella siphonifera* (d'Orbigny). Marine Micropaleontology, 35(3), 141-160, doi:10.1016/S0377-8398(98)00017-6.

Bouvier-Soumagnac, Y., and J.-C. Duplessy (1985), Carbon and oxygen isotopic composition of planktonic foraminifera from laboratory culture, plankton tows and Recent sediment: implications for the reconstruction of palcoclimatic conditions and of the global carbon cycle, Journal of Foraminiferal Research, 15, 302-320.

Boyle, E.A. (1981), Cadmium, zinc, copper, and barium in foraminifera tests. Earth and Planetary Science Letters, 53(1), 11-35.

Boyle, E. A. (1983), Manganese carbonate overgrowths on foraminifera tests. Geochimica et Cosmochimica Acta, 47(10), 1815-1819.

Brown, S. J., and H. Elderfield (1996), Variations in Mg/Ca and Sr/Ca ratios of planktonic foraminifera caused by postdepositional dissolution: Evidence of shallow Mg-dependent dissolution, Paleoceanography, 11(5), 543–551, doi:10.1029/96PA01491.

Chilingar, G. V. (1962), Dependence on temperature of Ca/Mg ratio of skeletal structures of organisms and direct chemical precipitates out of sea water. Bulletin of the Southern California Academy of Sciences, 61(1), 45-60.

Curray, J. R. (1991), Geological history of the Bengal geosyncline, Journal of Association of Exploration Geophysicists, 12(4), 209–219.

Curray, J. R., Emmel, F. J. and Moore, D. G. (2003), The Bengal Fan: morphology, geometry, stratigraphy, history and processes, Mar. Pet. Geol., 19(10), 1191–1223, doi:10.1016/S02648172(03)00035-7.

Dekens, P. S., Lea, D. W., Pak, D. K., and Spero, H. J. (2002), Core Top Calibration of Mg/Ca in Tropical Foraminifera: Refining Paleotemperature Estimation. Geochemistry, Geophysics, Geosystems 3, 4, 1-29.

Delaygue, G., Bard, E., Rollion, C., Jouzel, J., Stiévenard, M., Duplessy, J. C., & Ganssen, G. (2001), Oxygen isotope/salinity relationship in the northern Indian Ocean. Journal of Geophysical Research: Oceans, 106(C3), 4565-4574.

De Villiers, S. (2005). Foraminiferal shell-weight evidence for sedimentary calcite dissolution above the lysocline. Deep Sea Research Part I: Oceanographic Research Papers, 52(5), 671-680, doi:10.1016/j.dsr.2004.11.014.

Dittert, N., and Henrich, R. (2000), Carbonate dissolution in the South Atlantic Ocean: evidence from ultrastructure breakdown in Globigerina bulloides. Deep Sea Research Part I: Oceanographic Research Papers 47, 4, 603-620.

Duplessy, J.-C. (1982), Glacial to interglacial contrasts in the northern Indian Ocean. Nature (London, U. K.), 295(5849), 494–498, doi:10.1038/295494a0.

Eggins, S. M., Rudnick, R. L., and McDonough, W. F. (1998), The composition of peridotites and their minerals: a laser-ablation ICP–MS study. Earth and Planetary Science Letters, 154(1), 53-71, doi:10.1016/S0012-821X(97)00195-7.

Eggins, S., De Deckker, P., and Marshall, J. (2003). Mg/Ca variation in planktonic foraminifera tests: implications for reconstructing palaeo-seawater temperature and habitat migration. Earth and Planetary Science Letters, 212(3), 291-306.

Elderfield, H., and Ganssen, G. (2000). Past temperature and δ18O of surface ocean waters inferred from foraminiferal Mg/Ca ratios. Nature, 405(6785), 442-445, doi:10.1038/35013033.

Elderfield, H., Vautravers, M., and Cooper, M. (2002), The relationship between shell size and Mg/Ca, Sr/Ca, $\delta^{18}O$, and $\delta^{13}C$ of species of planktonic foraminifera. Geochemistry, Geophysics, Geosystems 3.8, 1-13.

Erez, J., Almogi-Labin, A. and Avraham, S. (1991): On the Life History of Planktonic Foraminifera: Lunar Reproduction Cycle in *Globigerinoides Sacculifer* (Brady), Paleoceanography, 6(3), 295–306, doi:10.1029/90PA02731.

Erez, J. (2003), The source of ions for biomineralization in foraminifera and their implications for paleoceanographic proxies. Reviews in mineralogy and geochemistry, 3, 54(1), 115-49.

Farmer, E. C., A. Kaplan, P. B. de Menocal, and Lynch-Stieglitz, J. (2007), Corroborating ecological depth preferences of planktonic foraminifera in the tropical Atlantic with the stable oxygen isotope ratios of core top specimens, Paleoceanography, 22, PA3205, doi:10.1029/2006PA001361.

Fehrenbacher, J. S., Spero, H. J., Russell, A. D., Vetter, L., and Eggins, S. (2015). Optimizing LA-ICP-MS analytical procedures for elemental depth profiling of foraminifera shells. Chemical Geology, 407, 2-9, doi:10.1016/j.chemgeo.2015.04.007.

Fraile, I., M. Schulz, S. Mulitza, U. Merkel, M. Prange, and Paul, A. (2009), Modeling the seasonal distribution of planktonic foraminifera during the Last Glacial Maximum, Paleoceanography, 24, PA2216, doi:10.1029/2008PA001686.

France-Lanord, C., Schwenk, T., and Klaus, A. (2014), Bengal Fan: Neogene and late Paleogene record of Himalayan orogeny and climate: a transect across the Middle Bengal Fan. IODP Scientific Prospective, 354, doi:10.14379/iodp.sp.354.

France-Lanord, C., Schwenk, T., and Klaus, A. (2015), Expedition Summary vol. 354. IODP, initial results, in prep.

Ganssen, G. M., and Kroon, D. (2000), The isotopic signature of planktonic foraminifera from NE Atlantic surface sediments: implications for the reconstruction of past oceanic conditions. Journal of the Geological Society, 157(3), 693-699.

Guptha, M. V. S. (1997), Seasonal variation in the flux of planktic Foraminifera; sediment trap results from the Bay of Bengal, northern Indian Ocean. The Journal of Foraminiferal Research 27.1, 519.

(Hadley Center) The Met Office Hadley Center for Climate Change (2015), Observations Dataset http://www.metoffice.gov.uk/hadobs/en4/download-en4-0-2.html, The Met Office, Devon, UK.

Han, W., McCreary, J. P., and Kohler, K. E. (2001), Influence of precipitation minus evaporation and Bay of Bengal rivers on dynamics, thermodynamics, and mixed layer physics in the upper Indian Ocean. Journal of Geophysical Research: Oceans (1978–2012), 106(C4), 6895-6916.

Hübscher, C., Spiess, V., Breitzke, M., and Weber, M. E. (1997), The youngest channel levee system of the Bengal Fan: results from digital sediment echosounder data. Marine Geology, 141(1-4), 125–145, doi:10.1016/s0025-3227(97)00066-2.

(Iolite Software) The Iolite Project: software for laser ablation ICPMS (2016), http://iolite-software.com, School of Earth Sciences, University of Melbourne, Melbourne, AU.

Jochum, K. P., Weis, U., Stoll, B., Kuzmin, D., Yang, Q., Raczek, I., Jacob, D. E., Stracke, A., Birbaum, K., Frick, D. A., Günther, D. and Enzweiler, J. (2011), Determination of Reference Values for NIST SRM 610–617 Glasses Following ISO Guidelines. Geostandards and Geoanalytical Research, 35: 397–429, doi: 10.1111/j.1751-908X.2011.00120.x.

Kudrass, H.R., Hofmann, A., Doose, H., Emeis, K., and Erlenkeuser, H. (2001), Modulation and amplification of climatic changes in the Northern Hemisphere by the Indian summer monsoon during the past 80 k.y. Geology 29(1), 63-66. doi: 10.1130/0091-7613(2001) 029<0063.

Kroon, D., and Darling, K. (1995). Size and upwelling control of the stable isotope composition of *Neogloboquadrina dutertrei*, *Globigerinoides ruber* and *Globigerina bulloides*: examples from the Panama Basin and Arabian Sea. Oceanographic Literature Review, 10(42), 855.

Lea, D. W., T. A. Mashiotta, and H. J. Spero (1999), Controls on magnesium and strontium uptake in planktonic foraminifera determined by live culturing, Geochemica et Cosmochimica Acta, 63, 2369-2379. doi:10.1016/S0016-7037(99)00197-0.

Lea, D. W. (2003), Elemental and isotopic proxies of past ocean temperatures, in Treatise on Geochemistry: The Oceans and Marine Geochemistry, vol. 6, edited by H. Elderfield, 365–390, Elsevier, New York.

Levitus, S. E. (1982), Climatological atlas of the world ocean, NOAA Professional Paper 13, US Government Printing Office, Washington DC.

Lohmann, G. P. (1995). A model for variation in the chemistry of planktonic foraminifera due to secondary calcification and selective dissolution. Paleoceanography, 10(3), 445-457.

Lupker, M., France-Lanord, C., Lavé, J., Bouchez, J., Galy, V., Métivier, F., Gaillardet, J., Lartiges, B., and Mugnier, J.-L. (2011), A Rouse-based method to integrate the chemical composition of river sediments: application to the Ganga Basin. Journal of Geophysical Research: Earth Surface, 116(F4):F04012, doi:10.1029/2010JF001947.

Mashiotta, T. A., Lea, D. W. and Spero, H. J. (1999), Glacial–interglacial changes in Subantarctic sea surface temperature and δ18O-water using foraminiferal Mg, Earth and Planetary Science Letters, 170(4), 417–432, doi:10.1016/S0012-821X(99)00116-8.

Mathien-Blard, E., and Bassinot, F. (2009), Salinity bias on the foraminifera Mg/Ca thermometry: Correction procedure and implications for past ocean hydrographic reconstructions, Geochemistry, Geophysics, Geosystems, 10, Q12011, doi:10.1029/2008GC002353.

Marr, J. P., J. A. Baker, L. Carter, A. S. R. Allan, G. B. Dunbar, and H. C. Bostock (2011), Ecological and temperature controls on Mg/Ca ratios of *Globigerina bulloides* from the southwest Pacific Ocean, Paleoceanography, 26, PA2209, doi:10.1029/2010PA002059.

Michels, K. H., Kudrass, H. R., Hübscher, C., Suckow, A. and Wiedicke, M. (1998), The submarine delta of the Ganges–Brahmaputra: cyclone-dominated sedimentation patterns, Marine Geology, 149(1-4), 133–154, doi:10.1016/S00253227(98)00021-8.

Mohan, R., Shetye, S. S., Tiwari, M. and Anilkumar, N. (2015), Secondary Calcification of Planktic Foraminifera from the Indian Sector of Southern Ocean, Acta Geologica Sinica-English Edition, 89(1), 27-37.

Mucci, A. (1987), Influence of temperature on the composition of magnesian calcite overgrowths precipitated from seawater. Geochimica et Cosmochimica Acta, 51(7), 1977-1984.

Nürnberg, D., J. Bijma, and Hemleben, C. (1996), Assessing the reliability of magnesium in foraminiferal calcite as a proxy for water mass temperatures, Geochem. Cosmochim. Acta, 60, 803-814, doi:10.1016/0016-7037(95)00446-7.

Peterson, L. C., and Prell, W. L. (1985). Carbonate dissolution in recent sediments of the eastern equatorial Indian Ocean: preservation patterns and carbonate loss above the lysocline. Marine Geology, 64(3-4), 259-290, doi:10.1016/0025-3227(85)90108-2.

Pierson-Wickmann, A.-C., Reisberg, L., France-Lanord, C. and Kudrass, H. R. (2001), Os-Sr-Nd results from sediments in the Bay of Bengal: Implications for sediment transport and the marine Os record, Paleoceanography, 16(4), 435–444, doi:10.1029/2000PA000532.

Raymo, M.E., and Ruddiman, W.F. (1992), Tectonic forcing of late Cenozoic climate. Nature 359(6391):117-122, doi:10.1038/359117a0.

Regenberg, M., Nürnberg, D., Steph, S., Groeneveld, J., Garbe-Schönberg, D., Tiedemann, R., and Dullo, W. C. (2006). Assessing the effect of dissolution on planktonic foraminiferal Mg/Ca ratios: Evidence from Caribbean core tops. Geochemistry, Geophysics, Geosystems, 7(7), doi:10.1029/2005GC001019

Regenberg, M., Nürnberg, D., Schönfeld, J., and Reichart, G. J. (2007). Early diagenetic overprint in Caribbean sediment cores and its effect on the geochemical composition of planktonic foraminifera. Biogeosciences, 4(6), 957-973.

Regenberg, M., Steph, S., Nürnberg, D., Tiedemann, R., and Garbe-Schönberg, D. (2009). Calibrating Mg/Ca ratios of multiple planktonic foraminiferal species with $\delta^{18}O$-calcification temperatures: Paleothermometry for the upper water column. Earth and Planetary Science Letters, 278(3), 324-336, doi:10.1016/j.epsl.2008.12.019.

Richey, J. N., Poore, R. Z., Flower, B. P., & Hollander, D. J. (2012). Ecological controls on the shell geochemistry of pink and white *Globigerinoides ruber* in the northern Gulf of Mexico: Implications for paleoceanographic reconstruction. Marine Micropaleontology, 82, 28-37, doi:10.1016/j.marmicro.2011.10.002.

Rohling, E.J., Cooke, S. (1999), Stable oxygen and carbon isotopes in foraminiferal carbonate shells, Modern Foraminifera. Kluwer Academic Publ, Dordrecht, 239–258.

Rostek, F., Ruhland, G., Bassinot, F. C., Beaufort, L., Müller, P. J., and Bard, E. (1994). Fluctuations of the Indian monsoon regime during the last 170,000 years: evidence from sea surface temperature, salinity and organic carbon records. Global Precipitations and Climate Change (27-51). Springer Berlin Heidelberg.

Sadekov, A., Eggins, S. M., De Deckker, P., Ninnemann, U., Kuhnt, W., and Bassinot, F. (2009). Surface and subsurface seawater temperature reconstruction using Mg/Ca microanalysis of planktonic foraminifera *Globigerinoides ruber*, *Globigerinoides sacculifer*, and *Pulleniatina obliquiloculata*. Paleoceanography, 24(3), doi: 10.1029/2008PA001664.

Schott, F. A., Xie, S.-P. and McCreary, J. P. (2009), Indian Ocean circulation and climate variability, Reviews of Geophysics, 47(1), RG1002, doi:10.1029/2007RG000245.

Shackleton, N. J. (1974), Attainment of isotopic equilibrium between ocean water and the benthic foraminifera genus Uvigerina: Isotopic changes in the ocean during the last glacial.

Schmidt, G.A., Bigg, G. R., and Rohling, E. J. (1999), Global Seawater Oxygen-18 Database - v1.21, http://data.giss.nasa.gov/o18data.

Siegel, D.A. and Armstrong, R.A. (2002), Trajectories of sinking particles in the Sargasso Sea: modeling of statistical funnels above deep-ocean sediment traps (vol. 44, 1519–1997). Deep-Sea Research I 49, 1115–1116.

Singh, A., Jani, R. A., and Ramesh, R. (2010). Spatiotemporal variations of the $\delta^{18}O$–salinity relation in the northern Indian Ocean. Deep Sea Research Part I: Oceanographic Research Papers, 57(11), 1422 1431, doi:10.1016/j.dsr.2010.08.002.

Spiess, V., Hübscher, C., Breitzke M., Böke, W., Krell, A., von Larcher, T., Matschkowski, T., Schwenk, T., Wessels, A., Zühlsdorff, L., and Zühlsdorff, S. (1998), Report and preliminary results of R/V Sonne Cruise 125, Cochin Chittagong, 17.10–17.11.97. Ber. Fachber. Geowiss, Univ. Bremen, 123.

Spero, H. J. and D.W. Lea (1993), Intraspecific stable isotope variability in the planktic foraminifera Globigerinoides sacculifer: Results from laboratory experiments. Marine Micropaleontology 22, 3, 221-234, doi:10.1016/0377-8398(93)90045-Y.

Spero, H. J., and D.W. Lea. (1996), Experimental determination of stable isotope variability in Globigerina bulloides: implications for paleoceanographic reconstructions. Marine Micropaleontology 28, 3: 231-246, doi:10.1016/0377-8398(96)00003-5.

Stoll, H. M., Arevalos, A., Burke, A., Ziveri, P., Mortyn, G., Shimizu, N., and Unger, D. (2007), Seasonal cycles in biogenic production and export in Northern Bay of Bengal sediment traps. Deep Sea

Research Part II: Topical Studies in Oceanography, 54(5), 558-580, doi:10.1016/j.dsr2.2007.01.002.

Unger, D. (2003), Seasonality and interannual variability of particle fluxes to the deep Bay of Bengal: influence of riverine input and oceanographic processes. Deep Sea Research Part II: Topical Studies in Oceanography, 50, 5, 897-923.

Weber, M. E., Wiedicke-Hombach, M., Kudrass, H. R., & Erlenkeuser, H. (2003). Bengal Fan sediment transport activity and response to climate forcing inferred from sediment physical properties. Sedimentary Geology, 155(3), 361-381, doi:10.1016/S0037-0738(02)00187-2.

Wit, J. C., Reichart, G.-J., Jung, S. J. A, and Kroon, D. (2010), Approaches to unravel seasonality in sea surface temperatures using paired single-specimen foraminiferal $\delta^{18}O$ and Mg/Ca analyses, Paleoceanography, 25, PA4220, doi:10.1029/2009PA001857.

Yanai, M., Li, C., and Song, Z. (1992), Seasonal heating of the Tibetan Plateau and its effects on the evolution of the Asian summer monsoon. Journal of the Meteorological Society of Japan, 70(1B), 319-351.

Zaric, S. (2005), Planktic foraminiferal flux of sediment trap CBBT-88/89_trap, lower. doi:10.1594/PANGAEA.264641.

Zhisheng, A., Kutzbach, J. E., Prell, W. L., and Porter, S. C. (2001), Evolution of Asian monsoons and phased uplift of the Himalaya–Tibetan plateau since Late Miocene times. Nature, 411(6833), 62-66.
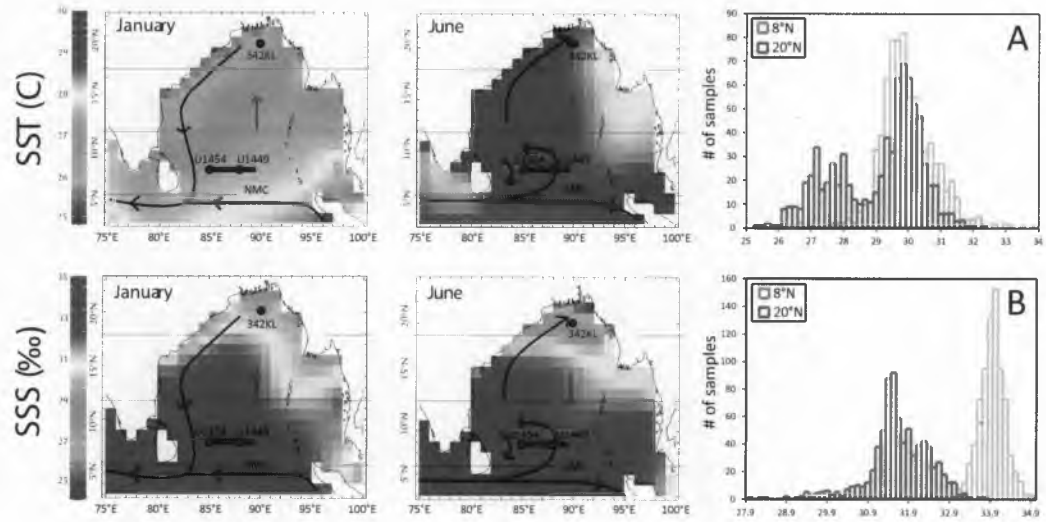
Figure 1. IODP Expedition 354 sites shown with a blue box, site U1454 (8.4°N, 85.5°E, 3721 m water depth) and U1449 (8.4°N, 88.7°E, 3653 m water depth) and site 342KL (20.6°N, 90°E, 1256 m water depth) shown as red circles [*France-Lanord et al.*, 2015]. Colorbar is modern SST and SSS. Black arrows are near-surface flow field and blue arrow is the sub-surface return flow during summer and winter monsoons; Southwest and Northeast Monsoon Currents (SMC and NMC) [*Levitus et al.*, 1994; *Schott*, 2009]. Panel A is seasonal distribution of SST and panel B is SSS for IODP Expedition 354 sites in light blue and 342KL site in grey [*Hadley Center*, 2015]. Seasonal variability is not normally distributed because the Southwest monsoon is more extreme than the Northeast monsoon.
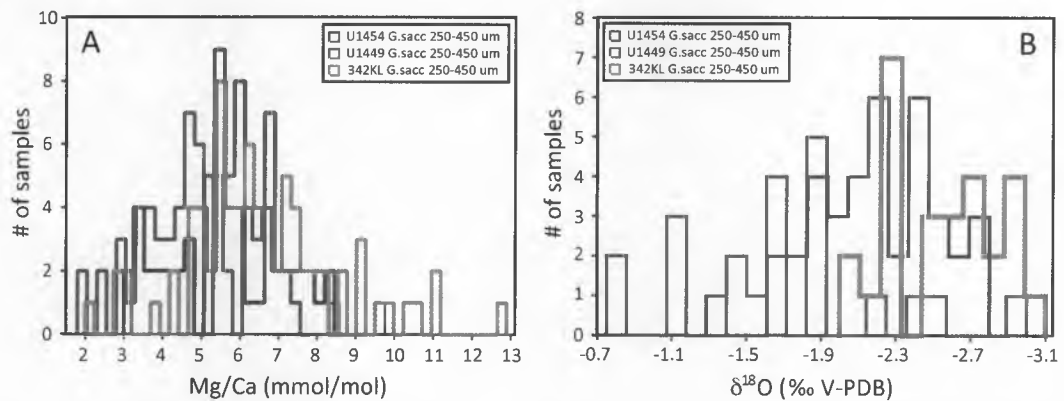
Figure 2. Histogram of Mg/Ca values (panel A) and $\delta^{18}O$ values (panel B) of *G. sacculifer* (250-450 μm) from site U1454 in red, site U1449 blue, and site 342KL in green. Mg/Ca values (mmol/mol) from site U1454 are significantly different from Mg/Ca values from sites U1449 and 342KL and Mg/Ca values from site U1449 are significantly different from site 342KL ($p < 0.01$, 2-sample student's t test, 2-tail). Variance is not statistically different from sites U1454 and U1449 ($p = 0.07$, F-test, 2-tail) and is statistically different between values from sites U1449 and 342KL ($p < 0.05$, F-test, 2-tail) and values from sites U1454 and 342KL ($p < 0.03$, F-test, 2-tail). $\delta^{18}O$ values from site U1454 are significantly different between sites U1449 and 342KL and $\delta^{18}O$ values from site U1449 are significantly different from site 342KL (p-value < 0.01, 2-sample student's t test, 2-tail). Variance of $\delta18O$ values from site U1454 is significantly different from site U1449 (p-value < 0.05, F-test, 2-tail) and variance of $\delta^{18}O$ values from site 342KL is not significantly different from site U1454 (p-value = 0.40, F-test, 2-tail) and is significantly different from site U1449 (p-value < 0.01, F-test, 2-tail).
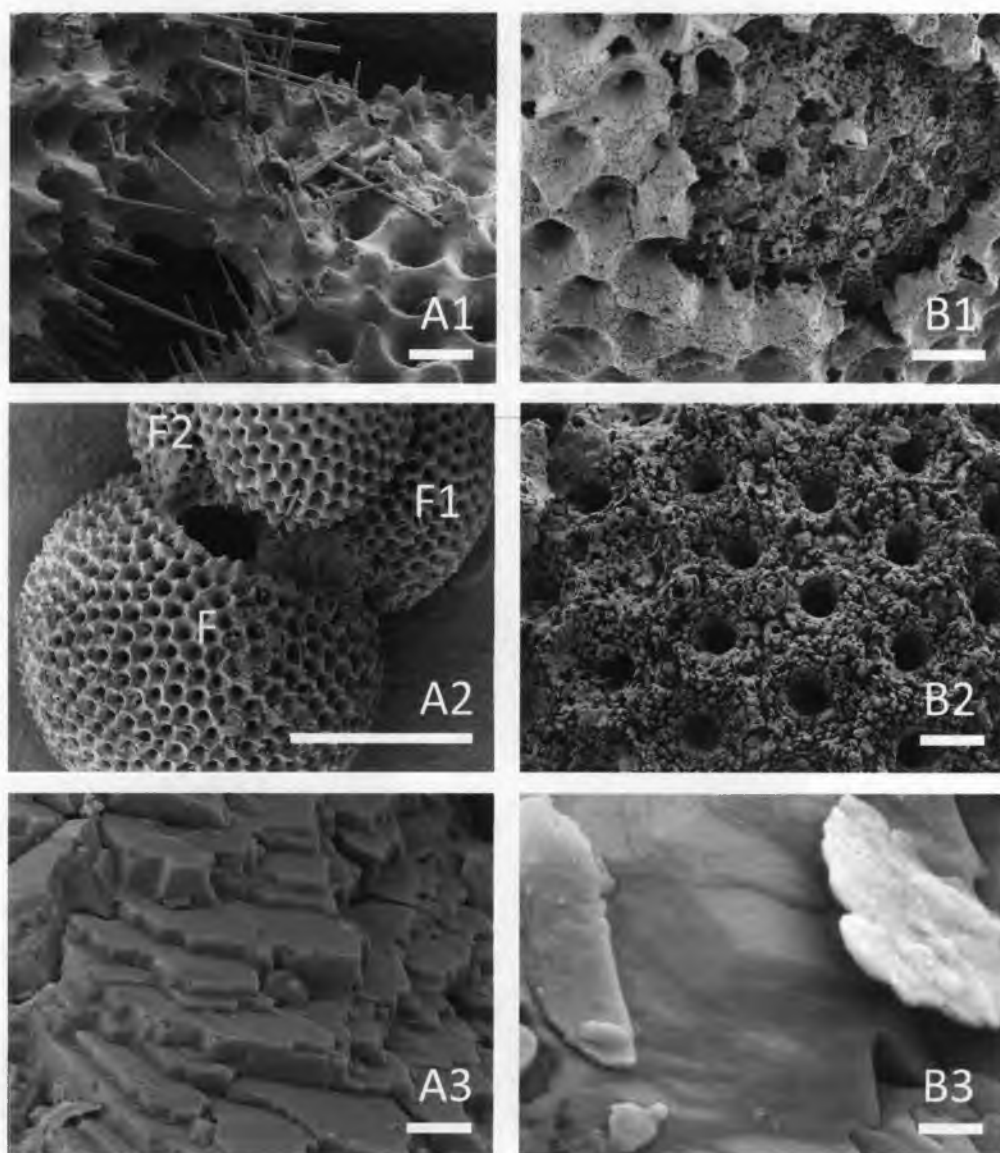
Figure 3. Scanning Electron Microscope images of *G. sacculifer* (250-450 μm) are well preserved from site U1454 in left panels (A1-A3) and less well preserved from site U1449 in right panels (B1-B3). A1: high spines and well-preserved spine bases, A2: rounded pores and high ridges, A3: sharp crystal edges, B1: sheeting surface layer, B2: partial dissolution and cracks of surface layer, B3: slightly rounded crystals. Scale bar in white is 10 μm (A1, A2 and B1, B2) and 100 nm (A3, B3). Panel A2 shows F, F1, and F2 chamber on an individual *G. sacculifer.*
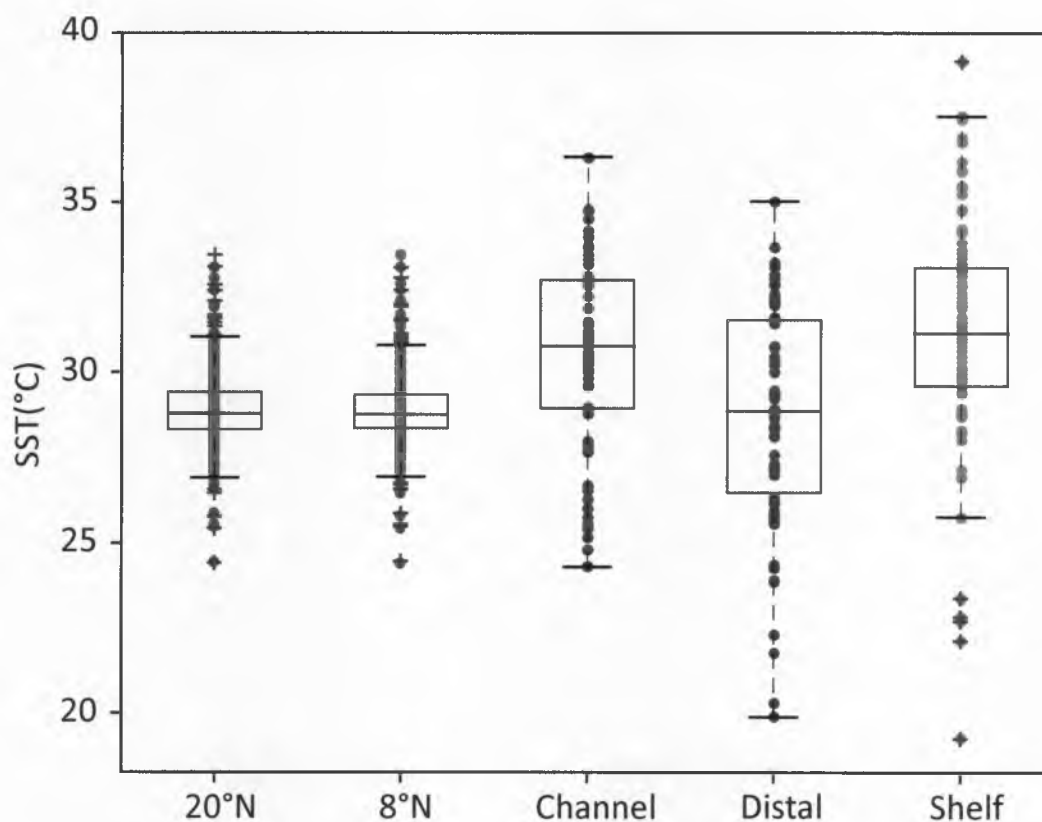
Figure 4. Distribution and boxplot (shows the mean as a red line, the 10th and 90th quantiles as blue lines, and outliers as a red cross) of modern SST values [*Hadley Center*, 2015] from 8°N in grey at IODP Expedition 354 locations, 20°N in light blue at 342KL site location and Mg/Ca SST estimates of *G. sacculifer* (250-450 μm) at site U1454 (in red), site U1449 (in blue), and 342KL (in green).We used the Anand et al. [2003] equation to convert Mg/Ca to temperature. SST_{insitu} from 8°N is significantly different from values from 20°N and from $SST_{Mg/Ca}$ values from all sites ($p < 0.01$, 2-sample student's t test, 2-tail). $SST_{Mg/Ca}$ values from site U1454 are statistically different from values from sites U1449 ($p < 0.02$, respectively, 2-sample student's t test, 2-tail) and $SST_{Mg/Ca}$ values from site U1449 and U1454 are statistically different from site 342KL ($p < 0.01$, 2-sample student's t test, 2-tail). $SST_{Mg/Ca}$ variance from site U1454 is statistically different from sites U1449 and 342KL ($p < 0.01$ and 0.02, respectively, F-test, 2 tail) and $SST_{Mg/Ca}$ variance from site U1449 are statistically different from site 342KL ($p < 0.01$, F-test, 2 tail).
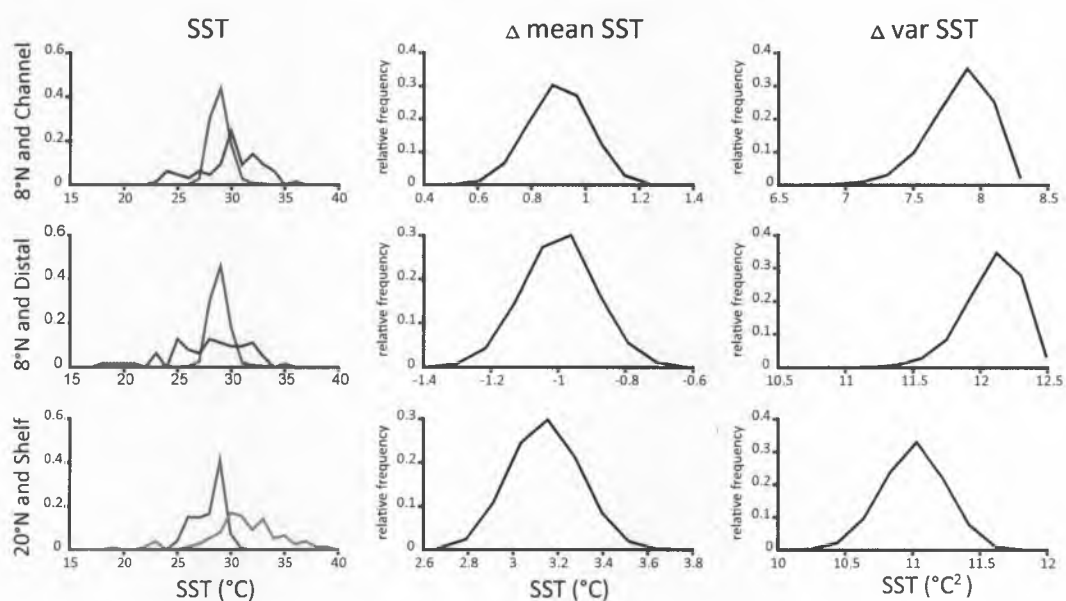
Figure 5. The left panels shows the $SST_{Mg/Ca}$ in grey and light blue and local oceanographic SST in color. The right panels shows the Δmean and Δvariance: the difference between the mean and variance of the $SST_{Mg/Ca}$ to SST_{MC}. The mean $SST_{Mg/Ca}$ from site U1449 is not statistically different from the SST_{MC} and the mean $SST_{Mg/Ca}$ from site U1454 records slightly warmer temperatures than SST_{MC}, while the mean $SST_{Mg/Ca}$ from site 342KL records much warmer temperatures than SST_{MC}.
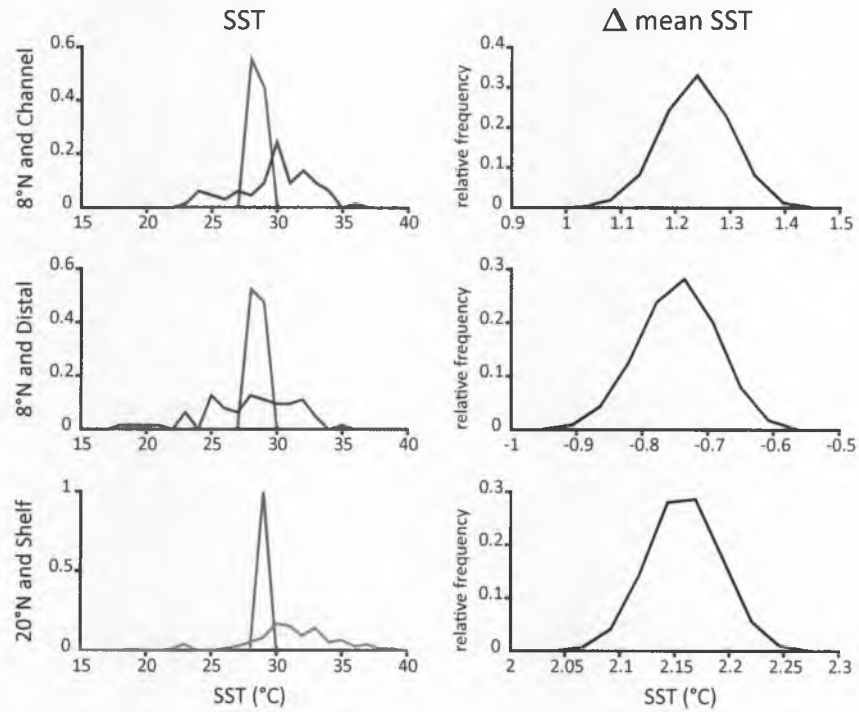
Figure 6. The left panels shows the $SST_{Mg/Ca}$ in grey and light blue and SST_{MC} in color created with a Monte Carlo simulation sampling just months where foraminifera are more abundent: May-August. The right panels shows the difference in the mean $SST_{Mg/Ca}$ and mean SST_{MC} (Δmean). The Δmean of values from site U1454 and site U1449 is not different from the previous simulation while Δmean of values from site 342KL is reduced using this seasonal sampling approach.
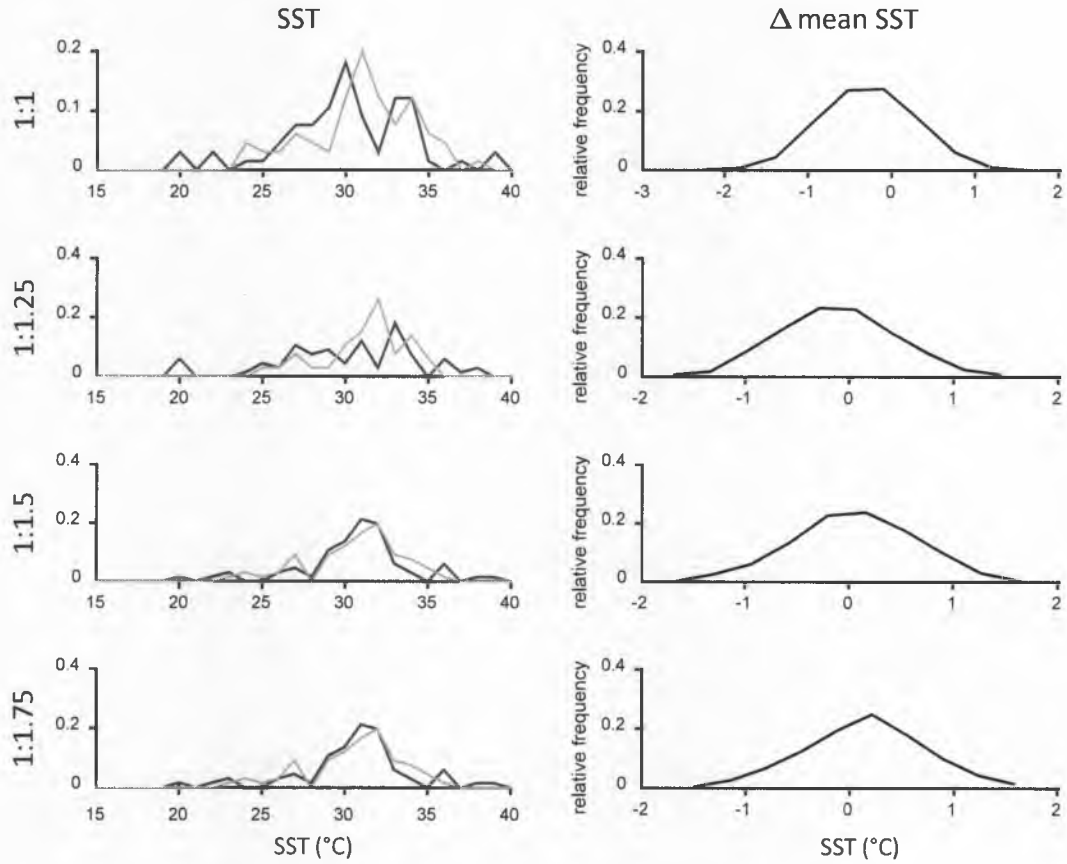
Figure 7. The left panels shows the $SST_{Mg/Ca}$ at sites U1454 in red and a Monte Carlo simulation created by randomly sampling from a portion of samples from site U1449 and a portion of samples from site 342KL in ratio specified on the y-axis. The right panels shows the distribution of Δmean: the difference between the mean of the $SST_{Mg/Ca}$ of site U1454 and the simulation. The Δmean is likely to be ~ 0°C when we sample from sites U1449 and 342KL in the proportion 1:1.5.
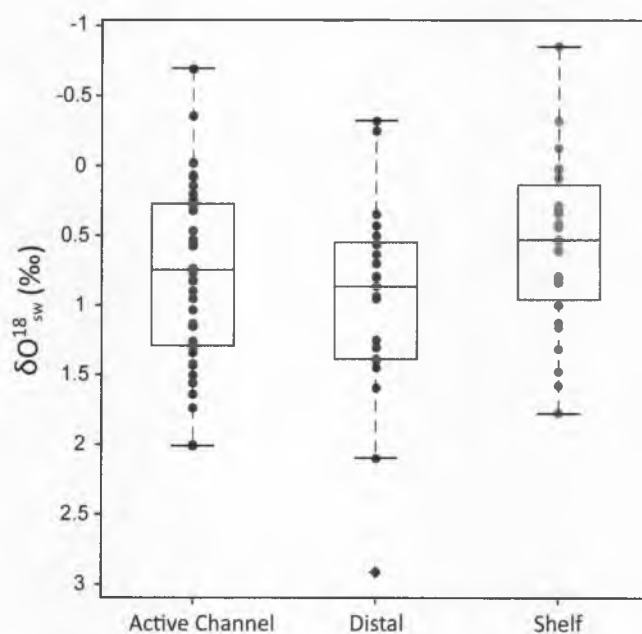
Figure 8. Distribution and boxplot of foraminifera derived $\delta^{18}O_{sw}$ from site U1454 in red, U1449 in blue, and 342KL in green. The mean of $\delta^{18}O_{sw}$ values from site 342KL is 0.24‰ less than that of site U1454 and 0.44‰ less than that of site U1449. The values from site U1454 are not significantly different from U1449 nor are they different from site 342KL (p = 0.28 and 0.15, respectively, 2-sample student's t test, 2-tail). Values from site 342KL are significantly different from site U1449 (p < 0.03, 2-sample student's t test, 2-tail).

Table 1. Sea surface salinity (SSS) and sea surface temperature (SST) range from January to June and mean values (± 1σ) from *Levitus* [1982] and *Hadley Center* [2015]. The oceanographic SST and SSS measured at site locations of IODP Expedition 354 and the 342KL northern site location have significantly different annual means ($p < 0.01$, 2-sample student's t test, 2-tail).

	Exp354 Sites	Site 342KL
Location	8°N	20°N
Jan SST (°C)	27.7	25.0
June SST	29.1	30.0
SST difference	1.4	5.0
Annual mean	29.0 ± 0.8	28.0 ± 1.4
Jan SSS (‰)	33.9	31.3
Jan SSS	33.2	29.3
SSS difference	0.7	2.0
Annual mean	33.9 ± 0.3	31.6 ± 0.8

Table 2. Mg/Ca (mmol/mol) and $\delta^{18}O$ (‰, V-PDB) mean values (± 1σ) of G. sacculifer (250-450 µm). N is the number of samples.

	U1454	U1449	342KL
Mg/Ca			
N	65	63	77
Mean	5.7 ± 1.4	4.9 ± 1.5	6.5 ± 2.0
$d^{18}O$			
Number of samples	37	20	27
Mean	-2.2 ± 0.3	-1.7 ± 0.5	-2.6 ± 0.3

Table 3. Comparison of several of the most commonly used calibration equations to convert Mg/Ca to SST (°C). Depth is 3721 m at site U1454 and 3653 m at site U1449 and ΔCO_3^{2-} at both sites is ~24 µmol/kg. Because of its shallow location, site 342KL is not corrected for depth or ΔCO_3^{2-}. SST reconstructed using the *Anand et al.* [2003] calibration equation most closely matches oceanographic SST at each sites.

	Calibration	Equation	U1454 mudline		U1449 mudline		354KL core-top	
			SST Mean	Mg/Ca SST - Oceanographic SST	SST Mean	Mg/Ca SST - Oceanographic SST	SST Mean	Mg/Ca SST - Oceanographic SST
Oceanographic SST			28.9 ± 0.9		28.9 ± 0.9		28.0 ± 1.4	
Mg/Ca SST	Anand et al. [2003] Multispecies (350 -500 µm)	Mg/Ca = 0.38exp0.090T	29.8 ± 2.9	0.9	27.9 ± 3.6	-1.0	31.1 ± 3.6	3.1
	Anand et al. [2003] with Regenberg [2006] depth correction	Mg/Ca = 0.38exp0.090[T+ (depth(m) − depth(critical)(m))]	30.5 ± 2.7	1.6	28.6 ± 3.3	-0.2	31.1 ± 3.6	3.1
	Regenberg et al. [2009] G. sacculifer (355-400 µm)	Mg/Ca = 0.60exp0.075T	29.7 ± 3.5	0.8	27.4 ± 4.3	-1.5	31.3 ± 4.3	3.3
	Elderfield and Ganssen [2000] Multispecies (350 -500 µm)	Mg/Ca = 0.52exp0.10T	23.7 ± 2.6	-5.2	22.0 ± 3.2	-6.9	24.9 ± 3.2	-3.1
	Dekens et al. [2002] G. sacculifer (250-350 µm) Depth corrected (Atlantic)	Mg/Ca = 0.37exp0.09[T- 0.36 (depth(km))]	31.2 ± 2.9	2.5	29.5 ± 3.6	0.6	31.4 ± 3.6	3.4
	Dekens et al. [2002] G. sacculifer (250-350 µm) [CO3^2-] corrected	Mg/Ca = 0.31exp0.84[T+0.048 (ΔCO3^2-)]	33.2 ± 3.2	4.3	31.2 ± 3.8	2.3	33.4 ± 3.6	5.4

Table 4. Oceanographic SST [*Hadley Center*, 2015] and $SST_{Mg/Ca}$ (°C) values of *G. sacculifer* (250-450 µm) converted to temperature using the calibration equation of *Anand et al.* [2003]. Oceanographic SST is 780 data points (60 years of monthly data).

	8°N	20°N	U1454	U1449	342KL
N	780	780	65	63	79
Mean and Std dev	29.0 ± 0.8	28.0 ± 1.4	29.8 ± 3.2	27.9 ± 3.7	31.1 ± 3.5

7. Appendices

Appendix A: Core descriptions

We recovered foraminifera for oceanographic analysis at International Ocean Drilling Program (IODP) Expedition 354 site U1454B (referenced as U1454), which is located on what is thought to be the western levee of the active channel (8.4°N, 85.5°E, 3721 m water depth), and site U1449A (referenced as U1449), which is ~250 km from channel activity (8.4°N, 88.7°E, 3653 m water depth) [Figure 1; *France-Lanord et al.*, 2014]. We compare data from the two IODP sites to site 342KL on the upper continental shelf of Bangladesh ~200 km south of the Ganges-Brahmaputra mouth (19°97'N, 90°03'E, 1256 m water depth) [*Pierson-Wickmann et al.*, 2001].

The top unit (7 m) of the core collected at site U1454 is different from all other cores and recovers a full levee sequence thought to be associated with modern channel activity [*France-Lanord et al.*, 2015]. Composition is dominated by repeated mud turbidites fining upward from silt to clay, coarser material thought to be associated with levee construction, and occasional plant fragments up to a few cm long, all indicating episodic high activity and contains foraminifera throughout [*France-Lanord et al.*, 2015]. Mud turbidites are between hemipelagic units, indicating episodic activity and times of inactivity. The top 20 cm of the core contains intervals of light brown-redish nanofossil rich calcareous clay (hemipelagic material with carbonate content from >2% to >80% with an average of 21% by weight) and indicates low activity and surprisingly contains no foraminifera. The mudline, which is the unconsolidated material sampled above this

sequence that represents the most modern sediment, is foraminifera rich. Because the lithology indicates turbidites and possible sediment transport, foraminifera may have washed in with sediments from further north.

The rate of modern sediment deposition at core site U1454 is estimated to be 56 cm/ka based on the average sedimentation rate from 0-70 m and the age model from Deep Sea Drilling Project (DSDP) site 218 (8.0°N and 86.3°E at 3743 m water depth, the same location as Expedition 354 site U1455) [*Curray et al.*, 2003]. Because of the nature of fan deposition sedimentation rates are highly variability and complicate age reconstruction. Lithologic, physical properties, seismic and geochronological data shows that sedimentation varies between cm/ka for hemipelagic units, representing an absence of fan sedimentation, and episodic sequences of >> 10 cm/ka when interlevee units form and levees rapidly build [*France-Lenord et al.*, 2015]. Although sedimentation rates are variable in the core sequence from 0-70 m used to create the age model and lower in the modern, it is likely that the mudline sample is < 1 ka [*France-Lenord et al.*, 2015].

The composition of the top unit (7 m) of core site U1449 is bioturbated nannofossil rich calcareous clay with black organic fragments and foraminifera, showing evidence of low activity and preservation [*France-Lanord et al.*, 2015]. The top unit of core site U1449 is very similar to all other Expedition 354 sites away from the active channel. These bioturbated units have relatively low deposition rates as the major source of particles is the settling of suspended sediment from the pelagic zone [*France-Lenord et al.*, 2015]. The rate of modern sediment deposition at core sites U1449 based on

estimates from DSDP site 218 is 56 cm/ka [*Curray et al.*, 2003]. Again this deposition rate is highly variable downcore with channel switching and transition from channel-levee activity to inactivity and lower in the modern, but mudline sample is likely < 1 ka [*France-Lenord et al.*, 2015].

The composition of core 342KL is sediment composed of hemipelagic mud that is not dominated by Ganges-Brahmaputra river sediment flux and is mostly composed of material derived from seawater and contains deposited foraminifera [*Pierson-Wickmann et al.*, 2001]. The lack of riverine sediments is a result of the strong westward currents at the mount of the Ganges-Brahmaputra river system diverting most of the riverine particle flux. The result is that riverine sediments transported through the active channel do not wash out pelagic sediments at core site 342KL. The rate of deposition in the core-top samples 0-3 cm at 342KL is ~ 5 cm/ka based on ages derived for each cm of the core [*Kudrass et al.*, 2001], so the samples are likely < 1 ka.

Appendix B: Foraminifera geochemical proxies

Measurements of $\delta^{18}O$ and Mg/Ca in foraminifera calcite reflect sea-water conditions at the time of shell formation and are used to reconstruct local SSS and SST [*Shackleton*, 1974; *Bemis et al.*, 1998; *Elderfield and Ganssen*, 2000]. The Mg/Ca SST proxy relies on the observation that the incorporation of Mg^{2+} ions is thermodynamic, so more Mg^{2+} ions are incorporated at higher temperature [*Chilingar*, 1962; *Mucci*, 1987] and the ratio of Mg to Ca increases exponentially with increased temperature [*Nürnberg*

et al., 1996; *Lea et al.*, 1999]. Although the Mg/Ca is thermodynamically effected, it is biologically controlled and therefore requires calibrations based on biogenic calcite [*Rosenthal et al.*, 1997]. Several calibrations are commonly used based on biogenic calcite collected in culturing, plankton tows, sediment trap, and core-top samples which each give a measurement of temperature sensitivity with some uncertainty (± 1.2-1.4°C) [*Elderfield and Ganssen, 2000*; *Dekens et al.* 2002; *Anand et al.*, 2003; *Regenberg et al.*, 2009].

$\delta^{18}O$ in foraminifera is defined by the ratio of ^{18}O to ^{16}O of seawater in which it grew to the ratio of ^{18}O to ^{16}O of Vienna Standard Mean Ocean Water (V-SMOW). The mass difference between water molecules that contain ^{18}O and those that contain ^{16}O cause physical and biological processes to partially separate water containing ^{18}O from water containing ^{16}O. Evaporation favors the lighter isotope and causes the local $\delta^{18}O$ of seawater to increase, while precipitation causes the local $\delta^{18}O$ to decrease. The ratio of ^{18}O and ^{16}O is a proxy for the difference between evaporation and precipitation, which affects local salinity [*Duplessy*, 1982]. As foraminifera form their shells, they fractionate and incorporate more ^{18}O than ^{16}O [*Shackleton*, 1974], and this fractionation increases as temperature decreases. This thermodynamic fractionation means that the $\delta^{18}O$ of foraminifera shells is offset from that of the water as a function of temperature. The $\delta^{18}O$ of planktonic foraminifera is influenced by global ice volume and the local salinity [*Shackleton*, 1974] and is therefore a combined signal of global seawater $\delta^{18}O$, local SSS, and SST [*Rohling and Cooke*, 1999].

Appendix C: Technical details of Mg/Ca analysis

Individual foraminifera were analyzed with laser ablation. Trace element profiles were obtained using a Teledyne/Photon Machines 193 nm ArF UV excimer laser with an ANU HelEx dual-volume laser ablation cell coupled to an Agilent 7700x quadrupole-ICP-MS. Ablated material is transported to the ICP-MS in a He-Ar gas mixture via a 10-path distributed delay manifold (a 'squid') that dampens laser pulse harmonics [*Eggins et al.*, 1998]. Gas composition and flow rate are determined by adjusting the flow of Ar and He as necessary to achieve high count rates on the sample/standard while maintaining ThO^+/Th^+ ratios less than 0.4% (tuned daily).

Between 3 to 7 laser spots were selected on each shell chamber where material was clean and unaltered by previous ablations. Element/Ca ratios for each data point were calculated using the software Iolite. We used Iolite software to screen for outliers and subtract average background counts (calculated with the laser off) by manually selecting laser noise between trace element profiles. The portion of the trace element profile area in which to integrate over is also manually selected using Iolite software.

Appendix D: Comparing Mg/Ca and $\delta^{18}O$ of different foraminifera species

Biological factors including species and chamber selection can introduce an uncertainty that exceeds the oceanographic signal [*Wit et al.*, 2010; *Sadekov et al.*, 2007; *Marr et al.*, 2011]. We measure Mg/Ca and $\delta^{18}O$ from sites U1454, U1449, and 342KL on different species (*G. sacculifer* and *G. ruber*) and chamber (F, F1, and F2) to quantify

the uncertainty. Mixed layer species *G. sacculifer* and *G. ruber* are thought to calcify in different water based on seasonal and depth habit preference related to nutrient availability and temperature [*Anand et al., 2002*; *Farmer et al.*, 2007]. *G. ruber* may prefer warmer water, live shallower in the water column (0-20 m vs. 20-75 m), and grow in warmer months than *G. sacculifer* and therefore record higher Mg/Ca and lower $\delta^{18}O$ values [*Farmer et al.*, 2007; *Fraile et al.*, 2009]. Because of its shallow habitat *G. ruber* has often been used to reconstruct SST [*Elderfield and Ganssen*, 2000; *Ganssen and Kroon*, 2000; *Anand et al.*, 2003]. However *G. ruber* may not be a reliable SST proxy in this study as *G. ruber* is more sensitive to salinity changes than *G. sacculifer* in the sub-tropics [*Nürnberg*, 1996; *Mathien-Blard and Bassinot*, 2009; *Arbuszewski et al.*, 2010] and a global foraminifera model indicates that *G. sacculifer* is the most reliable recorder of mean annual SST in low latitudes (20°N – 20°S) [*Fraile et al.*, 2009].

To identify the best species for this study we compared Mg/Ca between the two species (250-450 μm) from a southern site and the northern site. We compare 65 *G. sacculifer* and 20 *G. ruber* from site U1454 and 77 *G. sacculifer* and 13 *G. ruber* from site 342KL (Figure S1). *G. ruber* record a statistically significantly higher Mg/Ca than *G. sacculifer* at site U1454 (Table S1; $p < 0.0001$) and at site 342KL ($p = 0.0203$). $\delta^{18}O$ of 38 *G. sacculifer* have a mean that is lower than $\delta^{18}O$ of 6 *G. ruber* from site U1454 (Figure S1) and show no significant difference ($p = 0.2174$).

The *G. ruber* record of higher Mg/Ca and lower $\delta^{18}O$ than *G. sacculifer* in both the southern and northern sites is consistent with a warmer water preference of *G. ruber*.

The different between mean *G. ruber* and *G. sacculife*r Mg/Ca from sites U1454 and

342KL suggest a SST difference of 4.1°C and 2.4°C respectively using the calibration of

Anand et al. [2003]. This difference may be a result of the species depth habitat and is

consistent with the change in temperature through the water column (2°C and 3°C in top

75 m, respectively). Additionally the Mg/Ca derived SST difference may be influenced

by the species seasonal preference and is consistent with the seasonal temperature range

(1.4°C and 5.0°C, respectively; Figure 1). A year-long sediment trap collection deployed

in the central Bay of Bengal (13.15°N, 84.35°E, 2286 m water depth) indicates that the

largest flux of foraminifera is during the SWM during the warmest months (May -

August) accounting for 43% of *G. ruber* and 49% of *G. sacculifer* annual flux (Figure S7;

Zaric et al. 2005). This suggests that depth habitat plays a bigger role in the difference

between temperature records because there is no evidence in the sediment trap data that

suggests there is a difference in the seasonal preference between *G. ruber* and *G.

sacculifer*.

We choose to analyze sample groups of *G. sacculifer* in this study because they

more closely represent the oceanography of the study area. *G. ruber* record a mean

Mg/Ca that translates to temperature that is warmer than local SST at site U1454 and

342KL (5.0°C and 5.5°C respectively). Even when we apply a species specific calibration

G. ruber records warmer than local SST (2.1°C and 2.7°C, respectively). *G. sacculifer*

produces more realistic values and are more useful in this study as *G. ruber* samples are

sparse in the down-core record.

Chamber to chamber differences can account for a range of Mg/Ca [*Marr et al.*, 2011] and this variability is unique to the foraminifera species. For example previous single foraminifera studies show *G. ruber* may record a significantly different Mg/Ca ratio on F chambers than other chambers while no significant difference existed between the F chamber in individual *G. sacculifer* and the whole shell Mg/Ca ratio (p > 0.05) [*Wit et al.*, 2010; *Fehrenbacher*, in prep]. Variability between chambers shows that *G. sacculifer* F chamber records only slightly higher than mean shell Mg/Ca and is not statistically different (p = 0.8000) (Figure S4; Table S2). Because species have different depth habits, the Mg/Ca trend from F to F1 to F2 may be different for *G. sacculifer* and *G. ruber*. In addition to comparing Mg/Ca in *G. sacculifer* chambers we compare F, F1, and F2 chambers of 8 *G. ruber* from site 342KL to the three chamber mean. *G. ruber* F chamber records a mean value that is significantly lower than the chamber mean (p = 0.0270).

We find a significant increase in Mg/Ca from F to F1 to F2 chamber for *G. ruber* (Figure S4; Table S2). The lower Mg/Ca of the F chamber implies colder temperatures in the final life stage for *G. ruber*. Mg/Ca distribution (1σ) between chambers of an individual is 2.1 mmol/mol at site 342KL, which implies a temperature distribution (1σ) of 17.9°C for *G. ruber*. The magnitude of this distribution is larger than any temperature range an individual foraminifera would encounter during its life cycle at site 342KL due to seasonal range (5.0°C; Figure 1) or depth range (3°C in top 75 m) and suggest that variability between chambers may be a result of differences in Mg/Ca incorporation with

each ontogenetic state of *G. ruber*. Because the F chamber has significantly lower values than shell mean we are less confident in using single chambers of *G. ruber* for seasonal reconstruction.

Appendix E: Details on calcite dissolution correction

Foraminifera collect from Expedition 354 core sites may experience dissolution, which preferentially removes Mg^{2+} and shifts Mg/Ca SST estimates to colder temperatures [*Brown and Elderfield*, 1996; *Dekens et al.*, 2002]. Calibration equations that consider dissolution include a correction factor based on core depth or carbonate ion concentration at the site [*Dekens et al.*, 2002; *Regenberg et al.*, 2006]. We consider the depth correction of *Regenberg* [2006] to the multispecies (350-500 μm) *Anand et al.* [2003] equation:

$$Mg/Ca = 0.38 * e^{\,0.090 \,*\, [SST + (depth(m) - depth(critical)(m))]} \tag{1}$$

as well as the species specific (*G. sacculifer* 250-350 μm) depth corrected and ΔCO_3^{2-} corrected equations of *Dekens et al.*, [2002]:

$$Mg/Ca = 0.37 * e^{\,0.09 \,*\, [SST - 0.36 \,*\, (depth(km))]} \tag{2}$$

$$Mg/Ca = 0.31 * e^{\,0.84 \,*\, [SST + 0.048 \,*\, (\Delta CO_3^{2-})]} \tag{3}$$

Water ΔCO_3^{2-} values and depth correction were obtained from the GLODAP (Global Ocean Data Analysis Project) Ocean Carbon and WOCE (World Ocean Circulation Experiment) databases. ΔCO_3^{2-} is calculated using carbonate chemistry data (depth, temperature, salinity, alkalinity, CO_2, silicate and phosphate concentration) of the modern ocean from two sites closest to Expedition 354 sites: WOCE_I09N transect station 13270

(8°30'N, 85°59'E, water depth 3660 m) collected in March, 1995 and WOCE_101E

transect station 18992 (9°58'N, 88°24'N, water depth 3365 m) collected in October, 1995.

We calculated ΔCO_3^{2-} using the WOCE data for in situ carbonate ion concentration

(CO_3^{2-} [in situ]) and calcite saturation (ΩCa) and the CO_2 System Calculations Program

[*Lewis and Wallace,* 1998]. The difference in ΔCO_3^{2-} values between the two WOCE

sites (5.22 μmol/kg) corresponds to 0.13°C difference in the core top SST estimate using

the *Dekens et al.* [2002] ΔCO_3^{2-} corrected equations, and both yield SST estimates higher

than modern SST in the region.

Appendix F: Statistical approach

　　　　To test the hypothesis that two sample groups are equal to one another, such as

two groups of Mg/Ca values measured in foraminifera from different sites, we use a two

tailed two sample student's t-test. The t-test calculates the difference within each group,

determines the mean of these changes, and reports whether the mean of the differences is

statistically significant. This approach is used to derive the true mean (μ) of the

population and test if the two groups of foraminifera derived data are from the same

population and are therefore not likely to be distinct. The chance is α of getting the

critical value t to accept or reject the hypothesis that the two groups are the same and is

equal to:

$$(\bar{x} - \mu)/ S_{\bar{x}} \tag{4}$$

such that $S_{\bar{x}}$ is greater than $t_{\alpha,\upsilon}$, where $\bar{x}$ is the population mean, $S_{\bar{x}}$ is the standard error, and υ is the number of degrees of freedom (N - 1). The confidence interval we chose for α is 0.95. We choose a two tailed test as the relationship between the two groups of foraminifera derived data may be negative or positive.

To test the hypothesis that two sample groups have equal variances we use a two tailed F-test against the null hypothesis that the groups do not have equal variances. The test statistic F is equal to:

$$S_1{}^2 / S_2{}^2 \hspace{6cm} [5]$$

where $S_1{}^2$ and $S_2{}^2$ are the sample variances and the more this ratio deviates from 1, the stronger the evidence is that the variances are unequal. The critical value is

$$F_{\alpha,\ N1-1,N2-1} \hspace{6cm} [6]$$

where N1-1 and N2-1 are the degrees of freedom. The confidence interval we chose for α is 0.95. We choose a two tailed test as the variance of the first group may be greater or smaller than the variance of the second.
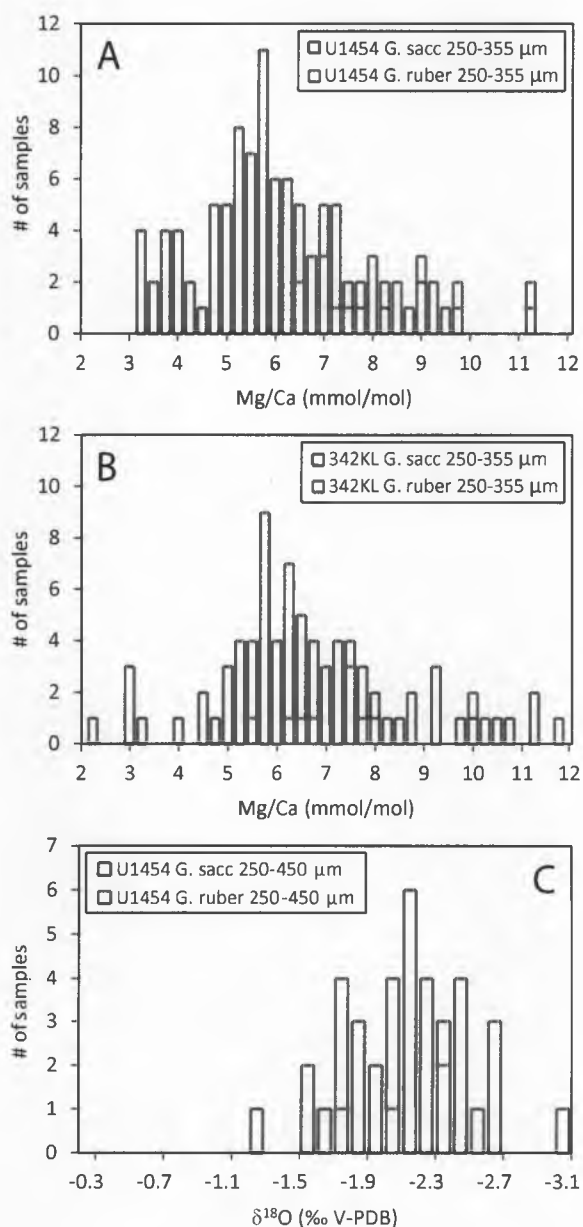
Figure S1. Histogram of Mg/Ca (mmol/mol) values of *G. sacculifer* (250-450 μm) in red and *G. ruber* (250-450 μm) in blue from site U1454 (panel A), site 342KL (panel B) and $\delta^{18}O$ (‰, V-PDB) values from site 342KL (panel C). Mg/Ca ratios are higher and $\delta^{18}O$ values are lower in *G. ruber* than values measured in *G. sacculifer*.
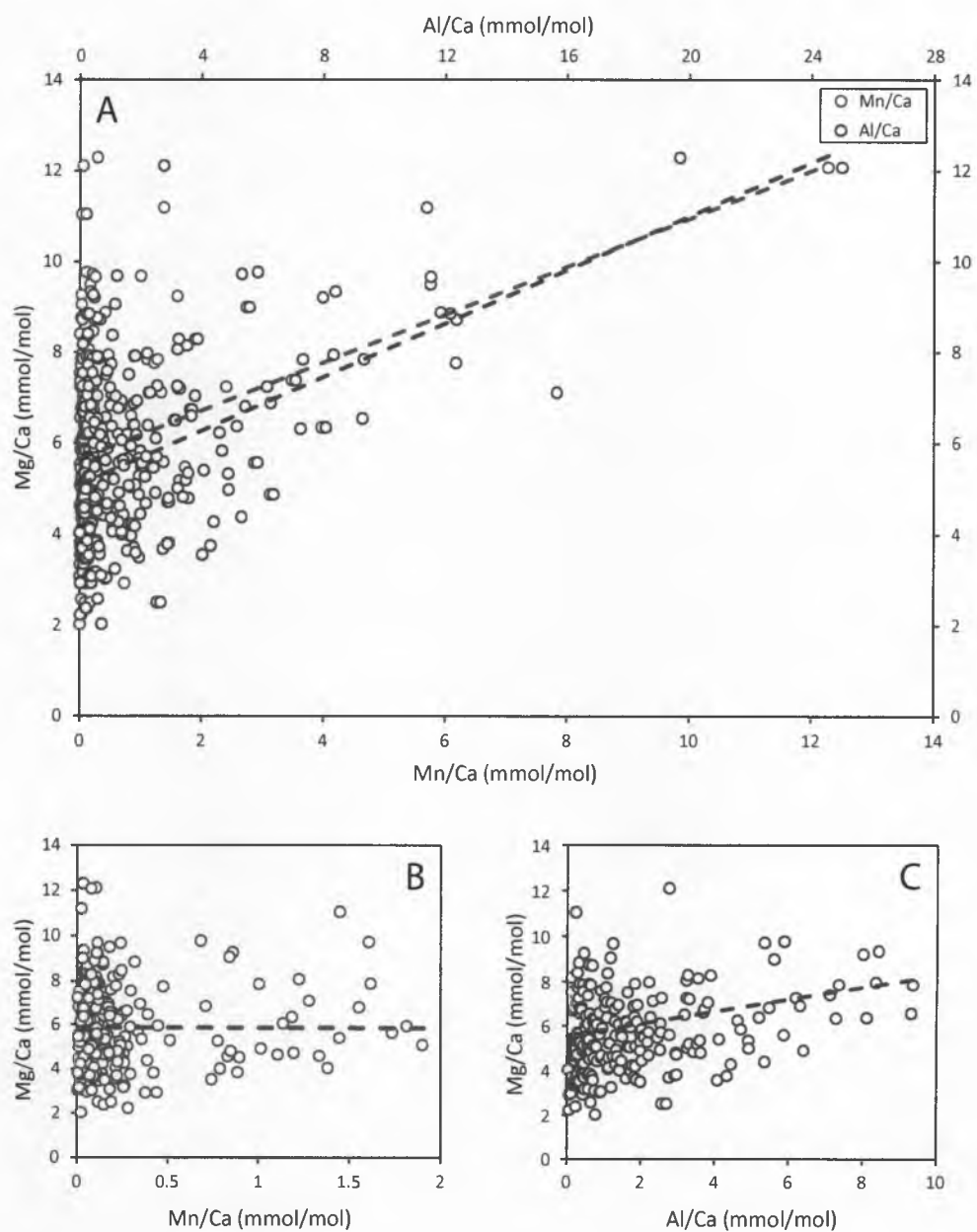
Figure S2. Panel A shows Mg/Ca plotted vs. Al/Ca in red and Mn/Ca in blue. The dashed colored lines represent a weak relationship between Al/Ca and Mg/Ca ($r^2 = 0.23$) and no relationship between Mn/Ca and Mg/Ca ($r^2 = 0.07$). When we remove samples > 10 mmol/mol Al/Ca there is no discernable trend ($r^2 = 0.09$, panel B) and when we remove samples > 2 mmol/mol from Mn/Ca there is no trend ($r^2 < 0.01$, panel C).
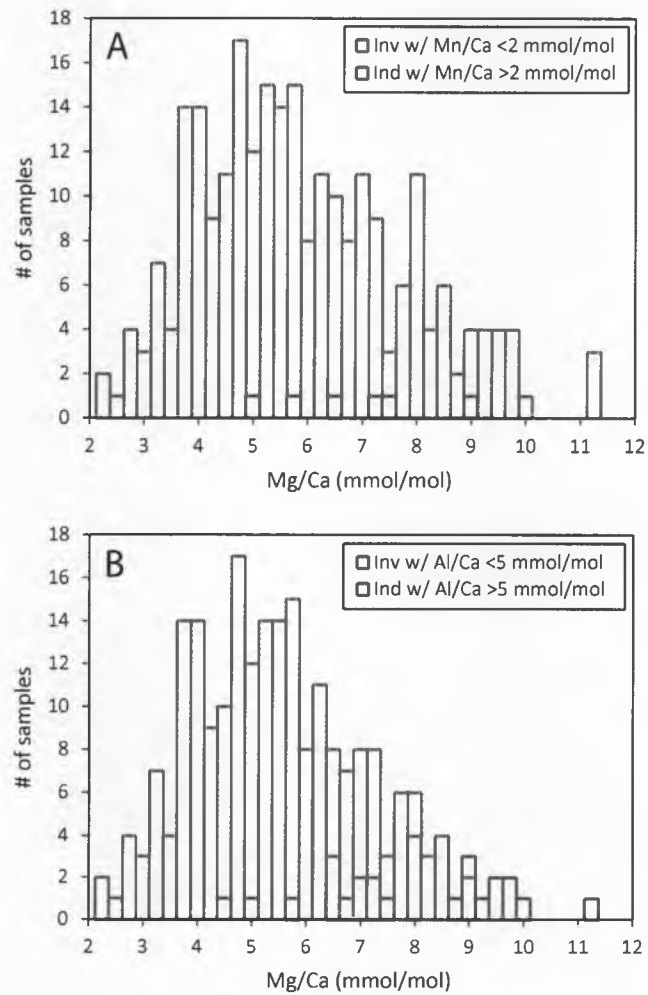
Figure S3. Panel A shows histogram of Mg/Ca ratios together with Mn/Ca ratios < 2 mmol/mol and > 2 mmol/mol. Higher Mn/Ca ratios do not record higher Mg/Ca ratios. Panel B shows histogram of Al/Ca ratios < 5 mmol/mol and > 5 mmol/mol. Higher Al/Ca ratios do record so highest values are excluded from this study.
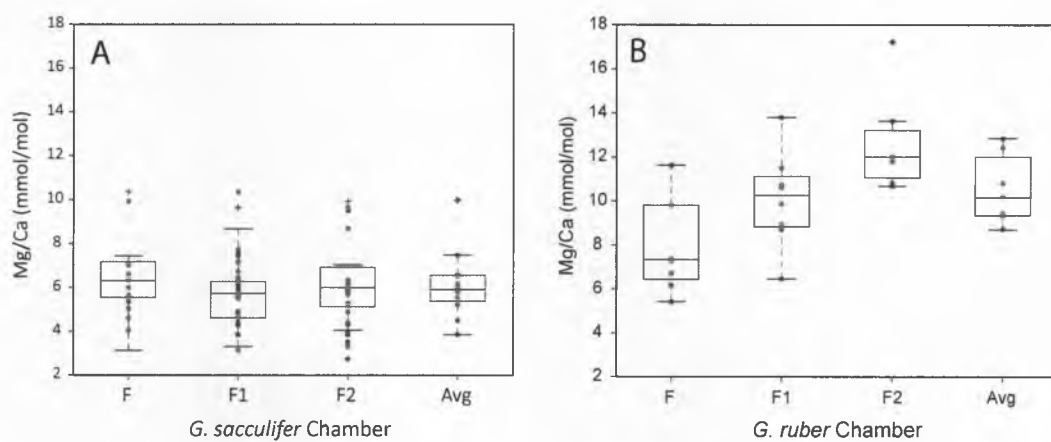
Figure S4. Distribution of Mg/Ca (mmol/mol) recorded by F, F1, and F2 chamber as well as chamber mean of individual *G. sacculifer* (panel A) and *G. ruber* (panel B) from site U1454 (in red), site U1449 (in blue), and site 342KL (in green). Boxplot shows the mean (as a red line), the 10th and 90th quantiles (as blue lines), and outliers (as a red cross). The boxplot is only created for site 342KL where all three chambers are measured. Mg/Ca measured in 12 *G. sacculifer* F chambers at site 342KL is not statistically different from the chamber mean (p = 0.80). 8 G. ruber F chambers at site 342KL have a measured Mg/Ca that is statistically different from the chamber mean (p < 0.03).
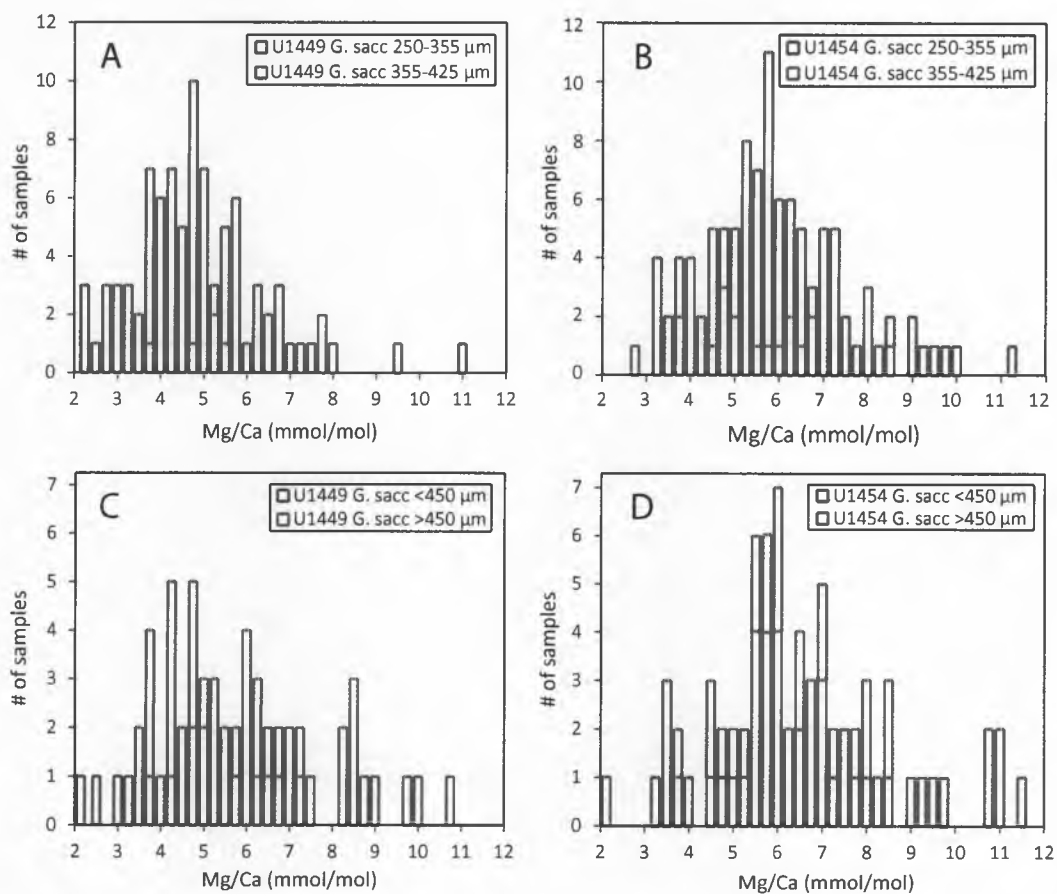
Figure S5. Panel A shows histogram of Mg/Ca (mmol/mol) *G. sacculifer* 250-355 μm in red and 355-425 μm in blue from site U1449 are not significant difference (p = 0.05). Panel B shows sizes 250-355 μm and 355-425 μm from site U1454 are also not significantly different (p = 0.37). Panel C shows histograms of *G. sacculifer* <450 μm in red and site U1454 *G. sacculifer* >450 μm in blue are significantly different at site U1449 (p < 0.01) and panel D shows sizes >450 um and <450 are statistically different at site U1454 (p < 0.01).
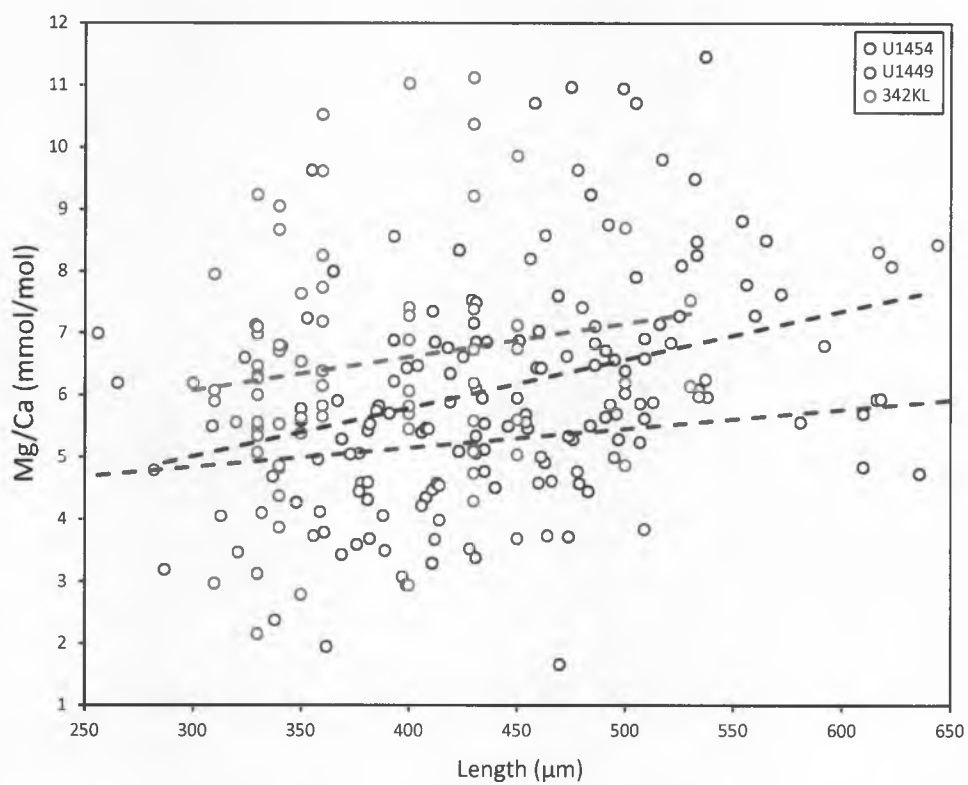
Figure S6. Mg/Ca (mmol/mol) plotted vs. length and separated by site, U1454 in blue, U1449 in red, and 342KL in green. The dashed colored lines represent a weak relationship between Mg/Ca and length from sites U1454, U1449, and 342KL (r^2 = 0.02, 0.09, and 0.10, respectively).
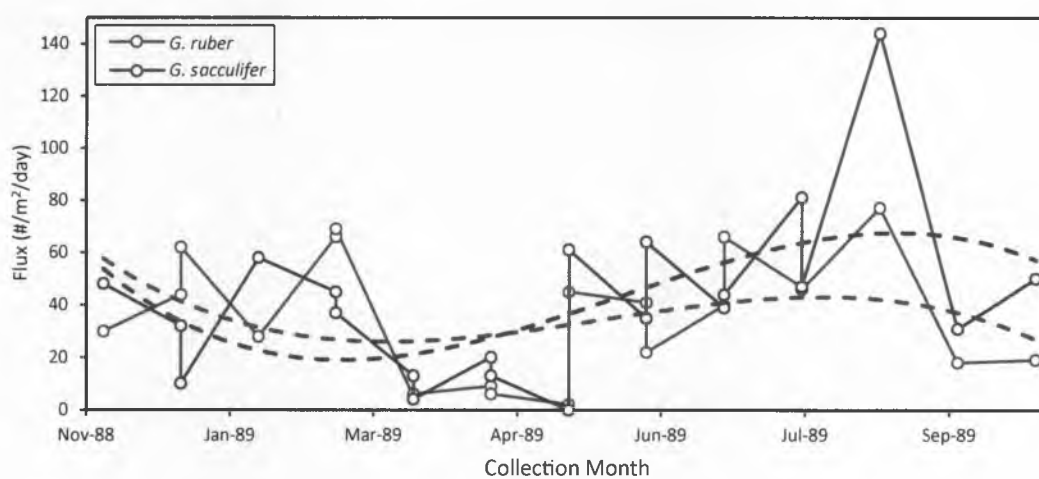
Figure S7. Fluxes of *G. ruber* in blue and *G. sacculifer* in red from the Central Bay of Bengal sediment trap (CBBT) collected at 13.15°N, 84.35°E measured in number of individuals/m²/day [*Zaric et al.*, 2005]. Samples were collected at 950 and 2286 m water depth every 27 days to resolve monthly fluxes. The yearlong trap is fit with a second order polynomial (*G. ruber* $r^2 = 0.12$; *G. sacculifer* $r^2 = 0.29$) which suggests an increase in foraminifera flux in May-August.

Table S1. Mg/Ca (mmol/mol) from sites U1454 and 342KL and $\delta^{18}O$ (‰, V-PDB) from site U1454 of *G. sacculifer* and *G. ruber*. *G. ruber* consistently record higher Mg/Ca and lower $\delta^{18}O$ reflecting warmer temperature.

		G. sacculifer	*G. ruber*
Mg/Ca U1454	# of samples	95	20
	mean	6.5 ± 2.0	8.0 ± 1.8
	p-value	<0.01	
Mg/Ca 342KL	# of samples	79	13
	mean	6.1 ± 1.7	8.1 ± 1.1
	p-value	0.02	
$\delta^{18}O$ U1454	# of samples	38	6
	mean	-2.2	-2.5
	p-value	0.22	

Table S2. F (final), F1 (next from final), F2 (two from final), and chamber mean (mean of F, F1, and F2) Mg/Ca (mmol/mol) from sites U1454, U1449, and 342KL measured on individual *G. sacculifer* and chamber values from site 342KL *G. ruber.*

		F	F1	F2	Chamber mean
G. sacculifer					
U1454	N	5			
	mean	4.7 ± 0.9	4.0 ± 1.2		
U1449	N	4			
	mean	6.5 ± 1.4	7.5 ± 2.5		
342KL	N	19		11	
	mean	6.3 ± 1.7	5.9 ± 1.8	6.2 ± 1.6	6.1 ± 1.5
G. ruber		8			
342KL	N				
	mean	8.0 ± 0.7	10.1 ± 0.7	12.6 ± 0.8	10.5 ± 0.8